AN ANALYSIS OF THE FACSIMILE-CAMERA RESPONSE TO RADIANT POINT SOURCES

by Friedrich O. Huck, Stephen J. Katzberg,
Daniel J. Jobson, and Carl L. Fales, Jr.

Langley Research Center
Hampton, Va. 23665

1. Report No. NASA TN D-7389	2. Government Accession No.	3. Recipient's Catalog No.
4. Title and Subtitle AN ANALYSIS OF THE FACSIMILE-CAMERA RESPONSE TO RADIANT POINT SOURCES		5. Report Date December 1973
		6. Performing Organization Code
7. Author(s) Friedrich O. Huck, Stephen J. Katzberg, Daniel J. Jobson, and Carl L. Fales, Jr.		8. Performing Organization Report No. L-9048
9. Performing Organization Name and Address NASA Langley Research Center Hampton, Va. 23665		10. Work Unit No. 815-20-04-03
		11. Contract or Grant No.
12. Sponsoring Agency Name and Address National Aeronautics and Space Administration Washington, D.C. 20546		13. Type of Report and Period Covered Technical Note
		14. Sponsoring Agency Code

15. Supplementary Notes

16. Abstract

   In addition to imaging the surrounding terrain, planetary lander cameras may also be used to survey the stars to aid in locating the lander site. The response of the facsimile camera, which was selected for the Viking lander missions to Mars, to a radiant point source is formulated and shown to result in a statistical rather than deterministic signal. The signal statistics are derived and magnitudes are evaluated for the brighter visual and red stars. The probability of detecting the resultant statistical signals in photosensor and preamplifier noise and the associated probability of false alarms are also determined.

17. Key Words (Suggested by Author(s)) Facsimile camera Radiant point sources Stars	18. Distribution Statement Unclassified – Unlimited		
19. Security Classif. (of this report) Unclassified	20. Security Classif. (of this page) Unclassified	21. No. of Pages 42	22. Price* Domestic, $3.00 Foreign, $5.50

AN ANALYSIS OF THE FACSIMILE-CAMERA RESPONSE
TO RADIANT POINT SOURCES

By Friedrich O. Huck, Stephen J. Katzberg, Daniel J. Jobson,
and Carl L. Fales, Jr.
Langley Research Center

SUMMARY

In addition to imaging the surrounding terrain, planetary lander cameras may also be used to survey the stars to aid in locating the lander site. The response of the facsimile camera, which was selected for the Viking lander missions to Mars, to a radiant point source is formulated and shown to result in a statistical rather than deterministic signal. The signal statistics are derived and magnitudes are evaluated for the brighter visual and red stars. The probability of detecting the resultant statistical signals in photosensor and preamplifier noise and the associated probability of false alarms are also determined.

INTRODUCTION

Although the primary purpose of the Viking lander imaging experiments on Mars is to visually characterize the landing sites, it will also be valuable to observe the brighter stars and planets. These observations could improve the accuracy of locating the landers, and, thus, aid in correlating Viking orbiter and lander science data (ref. 1).

A logical first step in preparation for such an experiment is to determine the response of the facsimile camera, which was selected for the Viking landers, to radiant point sources. At a first glance it may appear that this problem simply reduces to the detection of deterministic signals masked by noise. Actually, however, as will be shown, the facsimile camera generates a signal which is statistical rather than deterministic. This paper formulates and evaluates the facsimile-camera response to radiant point sources, the statistics of the resultant signals, and the probability of detecting the brighter visual and red stars in photosensor noise.

SYMBOLS

A_c camera objective lens aperture area, cm^2

ΔA_c elemental area of lens, cm^2

H	hypothesis
H_λ	spectral irradiance from point source, $W/cm^2\text{-}\mu m$
H_λ'	normalized spectral irradiance from blackbody radiator or Planckian emitter, μm^{-1}
I	signal current, A
i	integer
J_λ	spectral radiant intensity, $W/sr\text{-}\mu m$
K	magnitude of photosensor signal current, A
K'	normalized magnitude of photosensor signal current, A
k	peak spectral irradiance, pW/cm^2
L	lens-aperture point spread function
N	number of picture elements (pixels) per scan line
n	noise
P	probability
P_λ	spectral radiant power, $W/\mu m$
ΔP_λ	elemental spectral radiant power, $W/\mu m$
p	probability density
R_λ	spectral responsivity of photosensor, A/W
S	photosensor-aperture point spread function
s	signal

2

T	integration period of photosensor current, sec
T_S	sampling period of photosensor current, sec
t	time, sec
X	angular vertical sampling interval, rad
x	normalized period during which signal current is integrated (see eq. 6(c))
Y	angular azimuth sampling interval, rad
$\alpha = 1 - \beta$	(see eq. 6(a))
β	photosensor integration period normalized to the sampling interval X (see eq. 6(b))
Δ	magnitude of sampled signal, A-sec
δ	delta or impulse function
ζ	probability of detecting a star
η	normalized signal current threshold, A
$\theta(x)$	Heaviside step function, 1 for x > 0, and 0 for x $\leq$ 0
λ	wavelength, μm
ξ	probability of false alarm
ρ	angular radius of photosensor aperture, rad
σ	root-mean-square (rms) value of electronic noise current, A
τ	optical transmittance
χ	vertical angle of lens coordinates, rad (see fig. 2)

χ_S vertical angle of lens-mirror scanning coordinates, rad (see fig. 2)

$\Delta\chi$ vertical width of photosensor-aperture section, rad (see fig. 8)

Ψ_S angular azimuth stepping interval, rad

ψ azimuth angle of lens coordinate, rad (see fig. 2)

ψ_S azimuth angle of lens-mirror scanning coordinates, rad (see fig. 2)

$\Delta\psi$ azimuth width of photosensor-aperture section (see fig. 8)

ω angular distance between photosensor aperture and lens optical axis, rad

$\Pi(\chi)$ rectangular function, 1 for $\left|\chi\right| \leqq \frac{1}{2}$, and 0 elsewhere

$\text{III}(\chi)$ sampling or comb function, $\displaystyle\sum_{i=-\infty}^{\infty} \delta(\chi - i)$

Subscripts:

a   atmosphere

c   camera

n   noise

o   photosensor aperture

0   no star sample

1   one star sample

2   two star samples

1,2   at least one star sample

A bar over a symbol represents its average value.

A dot over a symbol represents the rate of motion.

ASSUMPTIONS

The analysis presented in this paper is subject to the following assumptions:

(1) The lens point spread function is small compared to the photosensor aperture and can be neglected. The constraints imposed by this assumption on the results of this paper, especially for the Viking lander camera, are discussed in appendix A.

(2) The photosensor-aperture shape is circular. Other photosensor-aperture shapes, which may often be preferable (ref. 2), would generate different signal statistics.

(3) A silicon photosensor is used.

(4) Only one point source, or star, with sufficient irradiance to be detectable is present within a selectable field of view, or set of image data.

IMAGING PROCESS

A basic configuration of the facsimile camera is illustrated in figure 1. Radiation from the object field is reflected by the scanning mirror, captured by the objective lens, and projected onto a plane which contains a photosensor aperture. The photosensor converts the radiation falling on the aperture into an electrical signal which is then amplified and sampled for digital transmission. As the mirror rotates, the imaged object field moves past the aperture, thus permitting the aperture to scan vertical strips. The camera rotates in small steps between each vertical line scan until the entire object field of interest is scanned. (In addition, the Viking facsimile camera has the capability of repeating vertical line scans in a fixed azimuth position.)

Two coordinate systems must be accounted for as illustrated in figure 2. One coordinate system with an origin at the center of the mirror (fig. 2(a)) accounts for the camera scanning geometry, and the other coordinate system with an origin at the center of the lens (fig. 2(b)) accounts for the imaging geometry. The vertical angle through which the mirror has scanned the object field is labeled $\chi_s = \dot{\chi}_s t$, where $\dot{\chi}_s$ is the mirror scanning rate, and the azimuth angle through which the camera has rotated is labeled ψ_s. The axis of azimuth rotation is also the optical axis of the objective lens and is labeled z in figure 2. The location of an object point (with the mirror optically unfolded) and the corresponding image point is measured as an angle from this common axis at the center of the objective lens. One angle, measured along the direction in which the imaged object field is moved by the scanning mirror, is labeled χ, and the other angle, measured normal to this direction, is labeled ψ. The angular location of the photosensor aperture is given by the angles χ_0 and ψ_0. It should perhaps be emphasized for clarity that the angles χ_s (fig. 2(a)) and χ (fig. 2(b)) occur in the same plane, but that the angles ψ_s (fig. 2(a)) and ψ (fig. 2(b)) occur in planes which are normal to each other. Since the
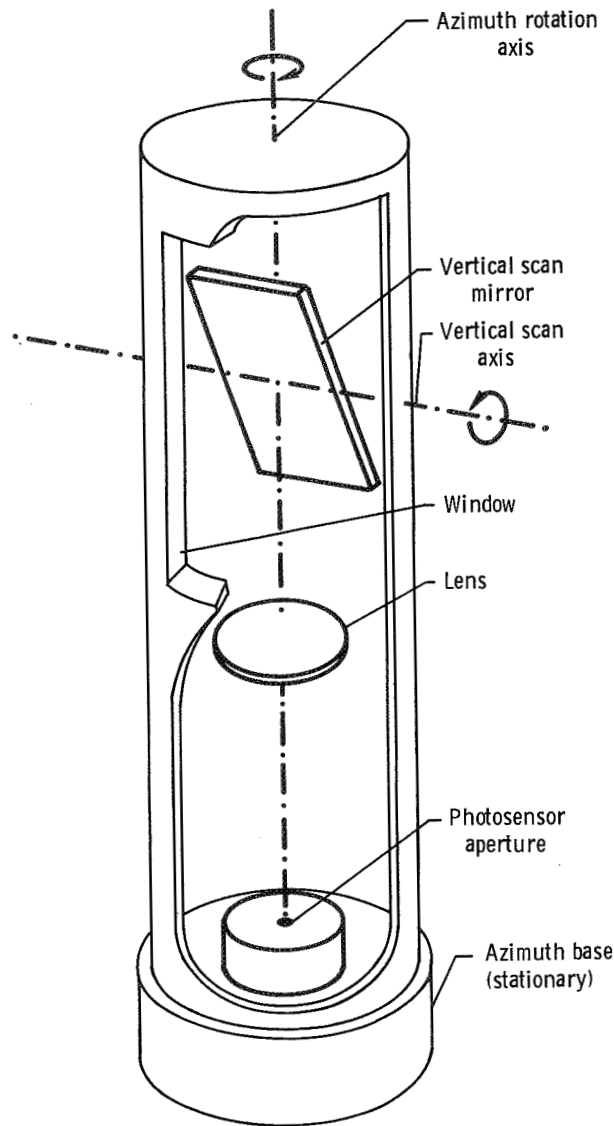
Figure 1.- Basic facsimile-camera configuration.

photosensor aperture is always located at or near the optical axis, only small (χ, ψ) angles are of interest; thus, $(\tan \chi, \tan \psi) \cong (\chi, \psi)$.

Let J_λ be the radiant intensity of a point source, and let $\delta(\chi, \psi)$ be the delta (ref. 3) or impulse (ref. 4) function. Then, as shown in figure 3, the elemental spectral radiant power ΔP_λ incident upon an elemental area of the camera lens ΔA_c is

$$\Delta P_\lambda = \frac{J_\lambda}{L^2} \tau_{a\lambda} \Delta A_c \cos \omega$$
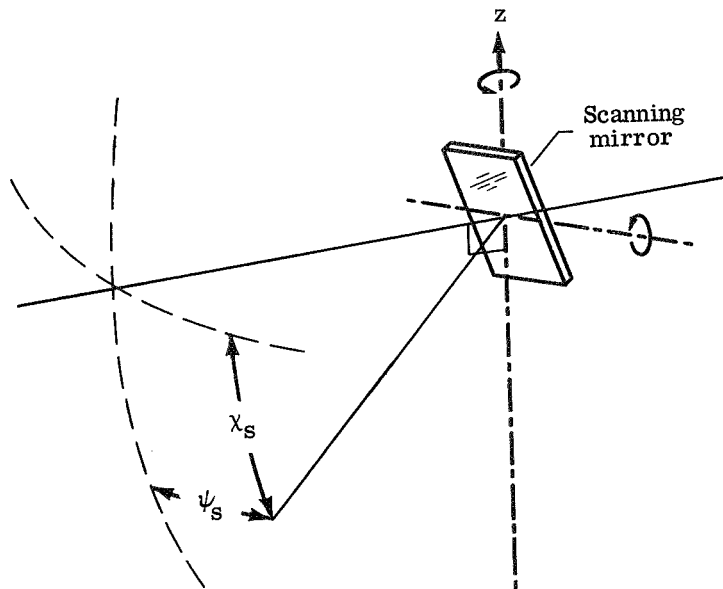
(a) Scanning geometry.
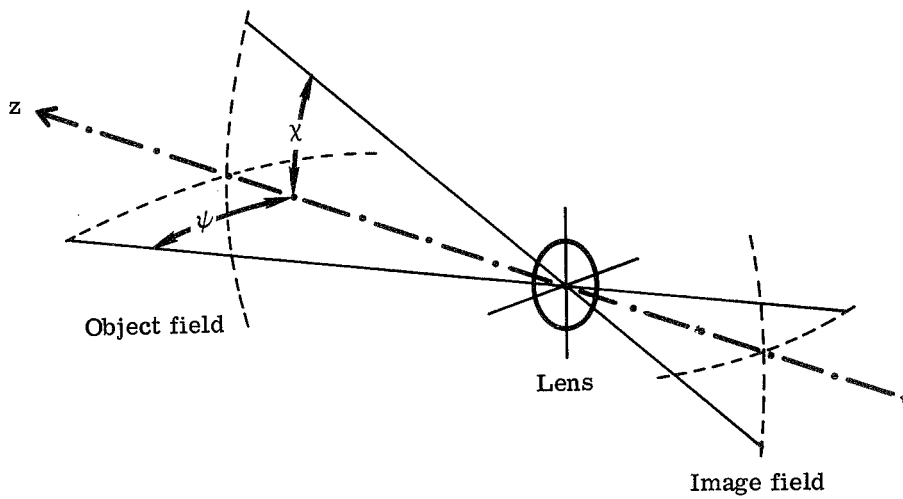
(b) Image-forming geometry.

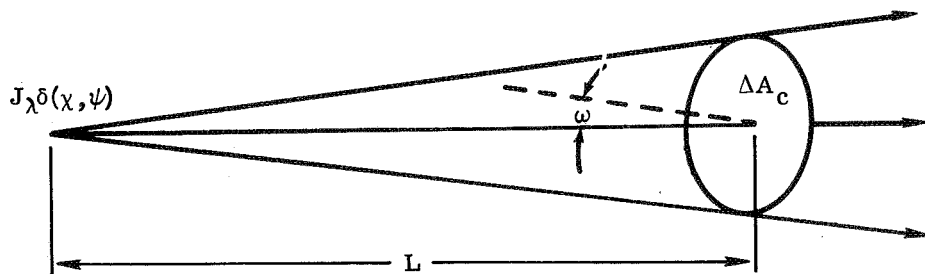Figure 2.- Camera coordinate system.

Figure 3.- Defining diagram for emitted and captured radiation.

where $\tau_{a\lambda}$ is the transmittance of the optical path between source and lens and $\omega \approx \sqrt{\chi^2 + \psi^2}$. Since the image of a point source must be near the optical axis in order to pass over the photosensor aperture (i.e., $\omega \approx 0$), and since the distance L of interest is great compared to the lens-aperture dimensions, ΔA_c may be replaced by the lens-aperture area A_c. Also, by substituting the spectral irradiance of the point source H_λ $\left(\text{where } H_\lambda = J_\lambda \big/ L^2\right)$ for its radiant intensity J_λ, the foregoing equation becomes

$$P_\lambda = A_c H_\lambda \tau_{a\lambda}$$

where ΔP_λ has been replaced by P_λ, the total spectral radiant power incident on the camera lens.

The transfer of the spectral radiant power of the point source which is captured by the objective lens $P_\lambda \, \delta(\chi,\psi)$ to the photosensor-aperture plane may be expressed by the convolution

$$\int_{-\infty}^{\infty}\int_{-\infty}^{\infty} P_\lambda \, \delta(\chi',\psi') \, L(\chi-\chi',\psi-\psi') \, d\chi' \, d\psi' = P_\lambda \, L(\chi,\psi)$$

where $L(\chi,\psi)$ is the lens point spread function. The effect of the scanning mirror is to shift the imaged radiant power over the photosensor-aperture plane, and the effect of the camera rotation between line scans is to advance the imaged radiant power in integral steps normal to the shifting direction. The process by which the photosensor converts this radiant power into an electrical signal may, therefore, be expressed by

$$I\left(\dot\chi_s t,\psi;\chi_0,\psi_0\right) = \int_0^\infty \int_{-\infty}^{\infty}\int_{-\infty}^{\infty} P_\lambda \tau_{c\lambda} R_\lambda \, L\left(\chi'-\dot\chi_s t,\psi'-\psi\right) S\left(\chi'-\chi_0,\psi'-\psi_0\right) d\chi' \, d\psi' \, d\lambda \, \frac{1}{Y} \, \text{Ш}\!\left(\frac{\psi'}{Y}\right)$$

$$(1)$$

where $\tau_{c\lambda}$ is the transmissivity of the optical path in the camera, R_λ is the responsivity of the photosensor, and $S(\chi,\psi)$ is the angular extent of the photosensor aperture.

The symbol $\text{Ш}(\psi/Y)$ is the sampling (ref. 3) or comb (ref. 4) function. This function is essentially an infinite sum of delta functions whose spacings in this case are related to the angular azimuth stepping interval Ψ_s by $Y = \Psi_s \cos \chi_s$ if χ_s is measured from a plane normal to the optical axis of the objective lens.

The photosensor-aperture shape is assumed to be circular and can be expressed as

$$S(\chi,\psi) = 1 \qquad \left(\begin{array}{c}|\chi| \lesssim \sqrt{\rho^2 - \psi^2}; \\ |\psi| \lesssim \sqrt{\rho^2 - \chi^2}\end{array}\right)$$

$$S(\chi,\psi) = 0 \qquad\qquad\qquad \text{(Elsewhere)}$$

where ρ is the angular radius of the aperture and is small.

The lens point spread function, or diffraction pattern, is assumed to be small compared to the photosensor aperture and can, therefore, be approximated by the impulse function; that is, $L(\chi,\psi) \approx \delta(\chi,\psi)$. Equation (1) becomes then

$$I\left(\chi_0,\psi_0;\dot\chi_s t,\psi\right) = \int_0^\infty P_\lambda \tau_{c\lambda} R_\lambda\, S\left(\dot\chi_s t-\chi_0,\psi-\psi_0\right)\, d\lambda\, \frac{1}{Y}\, \mathrm{III}\!\left(\frac{\psi}{Y}\right) = K\, S\left(\dot\chi_s t-\chi_0,\psi-\psi_0\right)\frac{1}{Y}\, \mathrm{III}\!\left(\frac{\psi}{Y}\right) \qquad (2)$$

where K is the magnitude of the signal current given by

$$K = \int_0^\infty P_\lambda \tau_{c\lambda} R_\lambda\, d\lambda = A_c\int_0^\infty H_\lambda \tau_{a\lambda}\tau_{c\lambda} R_\lambda\, d\lambda \qquad (3)$$

Equation (2) may be visualized with the help of figure 4 as presenting an infinite number of "tracks" of a point image, with spacing Y between successive tracks. These tracks generate a signal current $I\left(\chi_0,\psi_0;\dot\chi_s t,\psi\right) = K$ for the duration that a track crosses the photosensor aperture; otherwise, $I\left(\chi_0,\psi_0;\dot\chi_s t,\psi\right) = 0$.
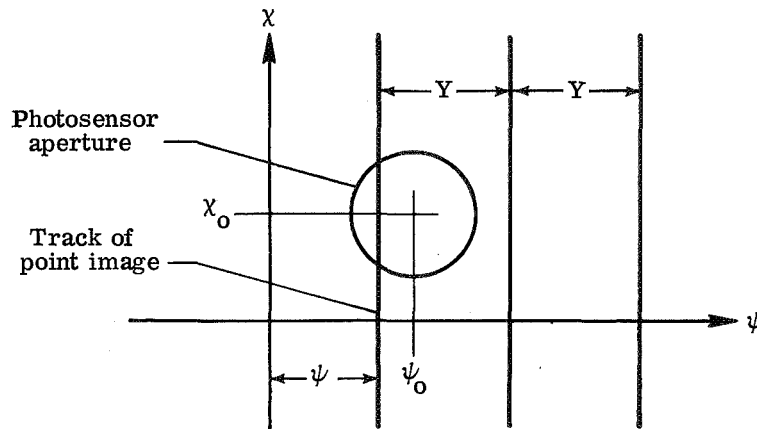

Figure 4.- Illustration of point-source image tracks in the photosensor-aperture plane.

The signal current is passed to a running mean integrator (ref. 5) for sampling — a process which may be formulated as follows: Let T be the period of signal integration so that $\dot{\chi}_s T$ becomes the effective angular interval over which integration occurs; and, similarly, let $T_S(>T)$ be the period of sampling so that $X = \dot{\chi}_s T_S$ becomes the effective vertical sampling interval. The sampled current may then be expressed as

$$I\left(\chi_0,\psi_0;\dot{\chi}_s T,\psi\right) = \frac{K}{X} \int_{\chi_s - \left(\dot{\chi}_s T/2\right)}^{\chi_s + \left(\dot{\chi}_s T/2\right)} S\left(\dot{\chi}_s t - \chi_0, \psi - \psi_0\right) d\dot{\chi}_s t \frac{1}{XY} \, \text{III}\left(\frac{\chi}{X}, \frac{\psi}{Y}\right) \qquad (4a)$$

or, by using the rectangular function

$$\Pi\left(\frac{\chi}{\dot{\chi}_s T}\right) = 1 \qquad\qquad\qquad \left(-\frac{\dot{\chi}_s T}{2} \leq |\chi| \leq \frac{\dot{\chi}_s T}{2}\right)$$

$$\Pi\left(\frac{\chi}{\dot{\chi}_s T}\right) = 0 \qquad\qquad\qquad\qquad\qquad \text{(Elsewhere)}$$

it can be expressed as

$$I\left(\chi_0,\psi_0;\dot{\chi}_s T,\psi_s\right) = \frac{K}{X}\left[S\left(\chi_0 - \chi, \psi_0 - \psi\right) * \Pi\left(\frac{\chi}{\dot{\chi}_s T}\right)\right] \frac{1}{XY} \, \text{III}\left(\frac{\chi}{X}, \frac{\psi}{Y}\right) \qquad (4b)$$

where $*$ represents the convolution operation.

Similarly, as before, this expression may be visualized with the help of figure 5 as presenting again an infinite number of tracks of a point image with spacing Y. However, although a signal current with magnitude K is generated for the duration that a track crosses the photosensor aperture, this current is integrated only during the interval $\dot{\chi}_s T$, once per sampling interval X. Consequently, the value of the sampled signal depends not only on the magnitude of the current generated by a point source but also on where and when the star image crosses the photosensor aperture, thus giving rise to a signal which is statistical rather than deterministic in nature.
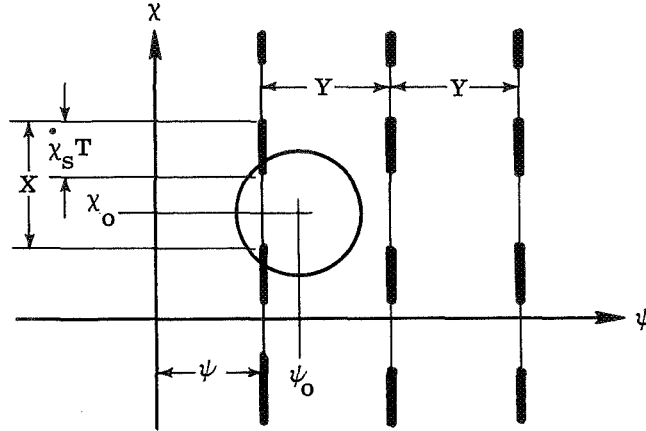
Figure 5.- Illustration of point-source image tracks and effective signal-integration intervals in the photosensor-aperture plane.

SIGNAL MAGNITUDE AND STATISTICS

The foregoing analysis has shown that the signal generated by a facsimile camera, when scanning a radiant point source, depends not only on the source irradiance and camera sensitivity but also on the camera scanning geometry, photosensor-aperture shape, and signal processing characteristics. This section determines the magnitude of the signal current generated by the brighter stars and the statistics of the sampled signal current.

Signal Magnitude

Reference 6 has shown that stars behave essentially as Planckian emitters (blackbody radiators), and that, therefore, the spectral irradiance for a star may be obtained from its visible radiance and effective temperature. In order to generalize results, it is convenient to rewrite equation (3) in the form

$$K' = \frac{K}{\tau_c A_c} = k \int_0^\infty H'_\lambda R_\lambda \, d\lambda \tag{5}$$

where K' is the signal current normalized with regard to optical design parameters of the facsimile camera (optical transmittance τ_c and lens-aperture area A_c), H'_λ is the normalized blackbody radiation, and k the peak spectral irradiance for a star. It is assumed that the atmosphere transmittance $\tau_{a\lambda}$ is unity, as is approximately true for the Martian atmosphere within the spectral responsivity of the silicon photosensor (except near the terminator), and that the camera transmittance $\tau_{c\lambda}$ is not wavelength dependent.
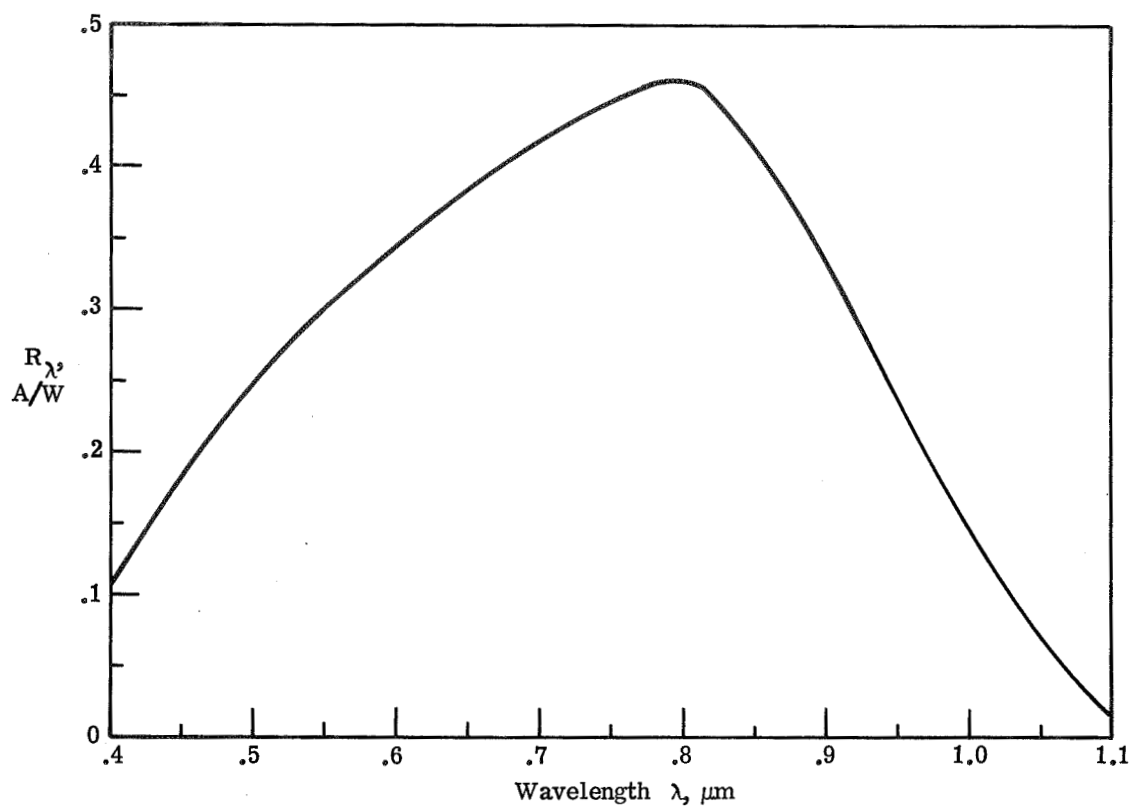
11

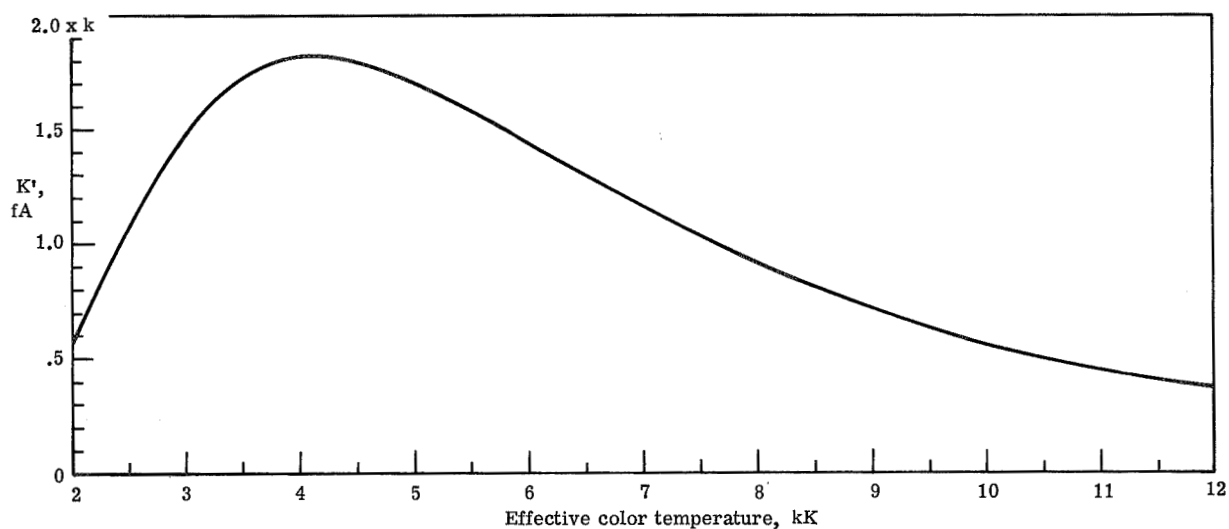Figure 6.- Spectral responsivity of silicon photosensor.

Figure 7.- Normalized photosensor signal current plotted against effective color temperature of a Planckian emitter.

The spectral responsivity of a typical silicon photosensor is plotted in figure 6, and the resultant photosensor current K' is plotted in figure 7. A list of the brightest visual and red stars for which the peak spectral irradiance k was calculated in reference 6 is given in table I, together with visual magnitude, effective temperature, and normalized photodiode current K'.

TABLE I.- CHARACTERISTICS OF THE BRIGHTEST VISUAL AND RED STARS AND
NORMALIZED SILICON PHOTOSENSOR SIGNAL CURRENT

Stars	Visual magnitude (a)	Effective temperature, K (a)	Peak spectral irradiance, k, pW/cm^2 (a)	Photosensor current, K', pA
Sirius	-1.60	11 200	40	1.21
Canopus	-.82	6 200	2.9	.28
Vega	.14	11 200	8	.24
Capella	.21	4 700	2.4	.30
Arcturus	.24	3 750	2.8	.35
Rigel	.34	13 000	9	.18
Achernar	.60	15 000	20	.27
Beta Centauri	.86	23 000	30	.10
Altair	.89	7 500	2.2	.16
Betelgeuse (variable)	.92	2 810	3.8	.36
Pollux	1.21	3 750	1.2	.15
Antares	1.22	2 900	2.3	.23
Alpha Crucis	1.61	2 810	3.2	.30
Mira (variable)	1.70	2 390	3.8	.26
Beta Gruis	2.24	2 810	1	.10
R. Hydrae (variable)	3.60	2 250	.8	.05

[a]Data taken from reference 6.

Signal Statistics

As is illustrated in figure 8, often only part of the signal current K is actually integrated and contributes to the sampled signal magnitude. Figure 8(a) depicts the photosensor aperture divided into rectangular sections of width $\Delta\psi$ and length $\Delta\chi_i$, and figure 8(b) shows two of these sections in more detail. The path of the star image across each one of the rectangular aperture sections is depicted by a thin line, and an arbitrarily selected integration period $\dot{\chi}_s T$ is depicted by a heavy line superimposed on each thin

line. It can be seen that either two, one, or no signals may be generated and that a signal may vary in magnitude from essentially zero to $K(\dot{\chi}_s T/X)$. The number of star signals obtained and their normalized magnitude (K = 1) depend on two independent events; namely, (a) where (along the azimuth direction) the star image passes across the photosensor aperture with respect to the aperture center, and (b) when (along the vertical scan direction) the star image passes across the photosensor aperture with respect to the time of signal current integration.

Within a single line scan, the signal current statistics of interest are the probability of generating two, one, or no signal, and the cumulative probability distribution, probability density, and average value of the integrated magnitude of the sum of two signals and of at least one signal. These statistics are presented here without derivation (analytical details are given in appendix B) and are based on the following assumptions and constraints:

(1) A star image may cross the photosensor aperture anywhere along azimuth with equal probability. Only one crossing is considered here; multiple crossings are considered in the next section.

(2) A star image may cross the photosensor aperture anytime with respect to the start of integration with equal probability.

(3) The angular vertical sampling interval X is assumed to be equal to the photosensor-aperture diameter 2ρ, as is generally the case.

In order to simplify the notation, it is convenient to make the following four definitions:

(1) The normalized period during which integration does not occur is given as

$$\alpha = \frac{X - \dot{\chi}_s T}{X} = 1 - \frac{\dot{\chi}_s T}{X} \tag{6a}$$
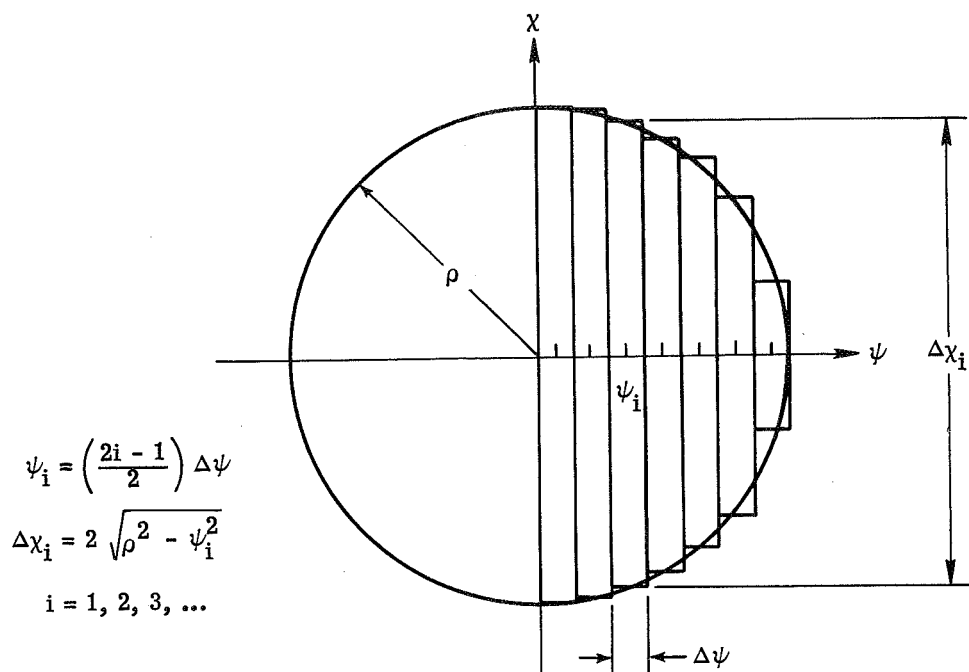
(2) The normalized period during which integration does occur is given as

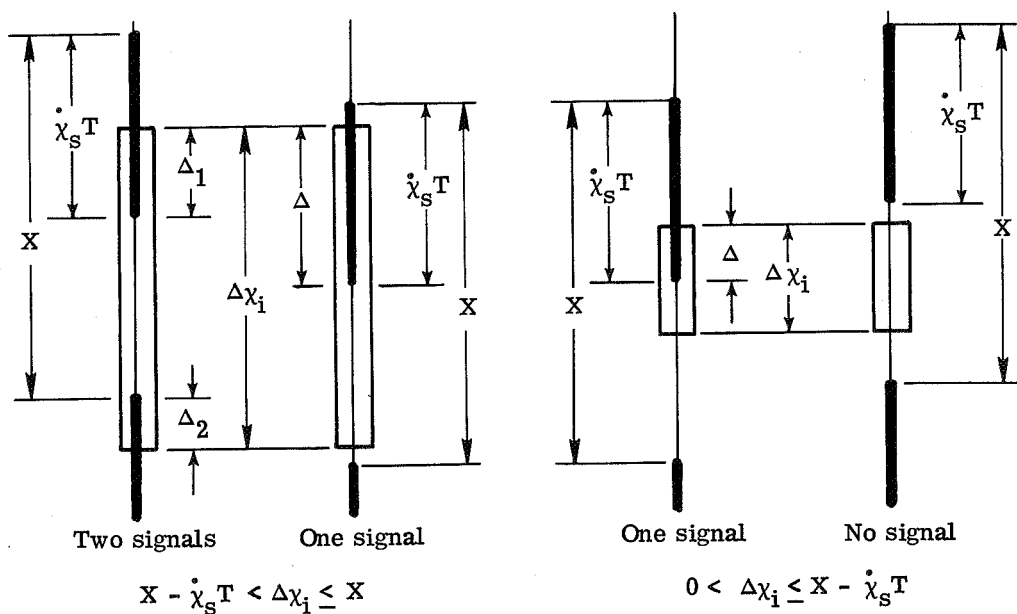$$\beta = \frac{\dot{\chi}_s T}{X} = 1 - \alpha \tag{6b}$$

(3) The normalized period during which integration occurs while the image of a point source is passing across the photosensor aperture is given as

$$x = c \frac{\dot{\chi}_s T}{X} = c\beta \tag{6c}$$

where $0 < c \leqq 1$; hence, $0 < x \leqq \beta$.

14

$$\psi_i = \left(\frac{2i-1}{2}\right)\Delta\psi$$

$$\Delta\chi_i = 2\sqrt{\rho^2 - \psi_i^2}$$

$$i = 1, 2, 3, \ldots$$

(a) Division of circular photosensor aperture into rectangular sections.

Two signals   One signal   One signal   No signal

$$X - \dot{\chi}_s T < \Delta\chi_i \leq X \qquad\qquad 0 < \Delta\chi_i \leq X - \dot{\chi}_s T$$

(b) Relation of signal integration and sampling intervals to aperture sections.

Figure 8.- Illustration for sampled signal-current statistics.

15

(4) A sampled signal normalized with respect to X is defined by the symbol Δ; if two signals are to be distinguished, they are noted as Δ_1 and Δ_2. The magnitude of a signal may vary, therefore, from zero to βK; that is, $0 < \Delta/K \leqq \beta$.

<u>Probability of signal generation.</u>- The probabilities of generating two, one, or no star signals are, respectively (see appendix B),

$$P_2\left\{\Delta_1{>}0, \Delta_2{>}0\right\} = \frac{1}{2}\left(\cos^{-1}\alpha - \alpha\sqrt{1-\alpha^2}\right) \tag{7a}$$

$$P_1\left\{\Delta{>}0\right\} = \frac{1}{2}\left(\frac{\pi}{2} + 2\beta + 2\alpha\sqrt{1-\alpha^2} - 2\cos^{-1}\alpha\right) \tag{7b}$$

$$P_0\left\{\Delta{=}0\right\} = \frac{1}{2}\left(2\alpha + \cos^{-1}\alpha - \frac{\pi}{2} - \alpha\sqrt{1-\alpha^2}\right) \tag{7c}$$

The probability of generating at least one star signal can be obtained from the previously given results as

$$P_{1,2}\left\{\Delta{>}0\right\} = P_2\left\{\Delta_1{>}0, \Delta_2{>}0\right\} + P_1\left\{\Delta{>}0\right\} = 1 - P_0\left\{\Delta{=}0\right\} \tag{7d}$$

Figure 9 illustrates the variation of these probabilities with the normalized integration period β.
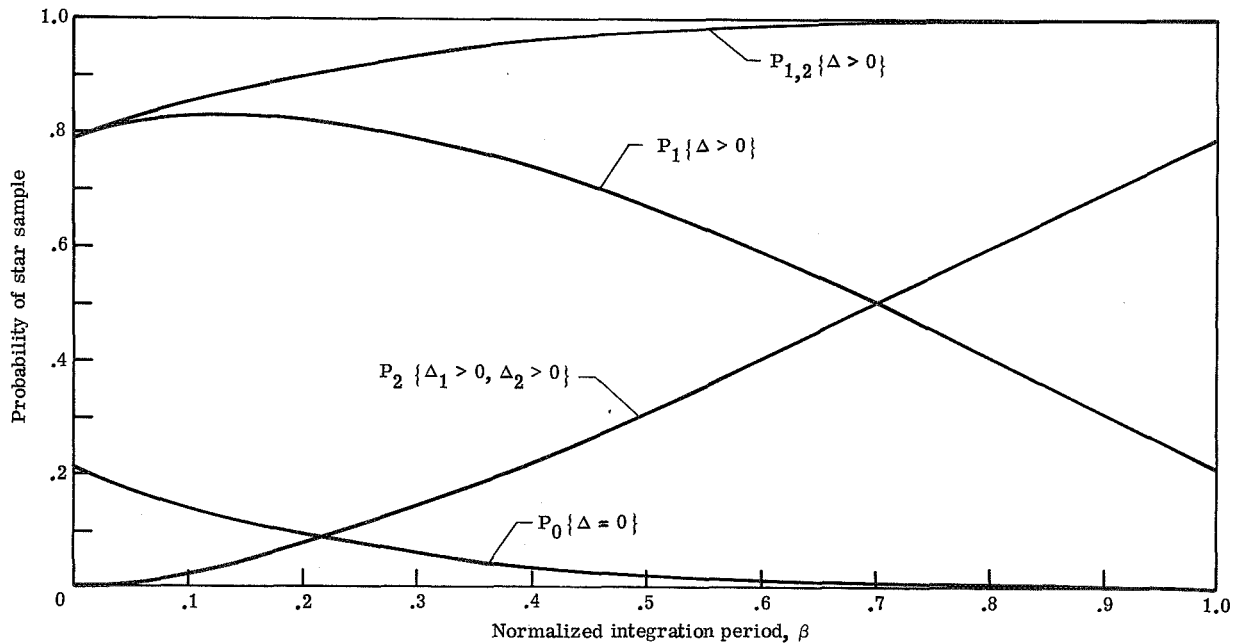

Figure 9.- Variation of the probability that two, one, at least one, or no signal sample is generated with normalized integration period β.

Cumulative probability distribution.- Two probability distributions are of interest (see appendix B) and are given as follows:

(1) The probability that the sum of two star samples, $\Delta_1 + \Delta_2$, is larger than xK is given as

$$P_2\left\{x<\left(\Delta_1+\Delta_2\right)\Big/K\leqq\beta\right\} = \frac{1}{2}\left[\cos^{-1}(\alpha + x) - (\alpha - x)\sqrt{1 - (\alpha + x)^2}\right] \tag{8a}$$

$$P_2\left\{\beta\leqq x<\left(\Delta_1+\Delta_2\right)\Big/K\right\} = 0 \tag{8b}$$

(2) The probability that at least one star signal, Δ_1 or Δ_2 or both, is larger than xK is given as

$$P_{1,2}\left\{x<\Delta/K\leqq\beta\right\} = \frac{1}{2}\left[\cos^{-1}x - \cos^{-1}(\alpha + 2x) + (2\beta - 3x)\sqrt{1 - x^2} + (\alpha + 2x)\sqrt{1 - (\alpha + 2x)^2}\right] \quad (x < \beta/2)$$

$$P_{1,2}\left\{x<\Delta/K\leqq\beta\right\} = \frac{1}{2}\left[\cos^{-1}x + (2\beta - 3x)\sqrt{1 - x^2}\right] \quad (\beta/2 \leqq x \leqq \beta) \tag{8c}$$

$$P_{1,2}\left\{\beta\leqq x<\Delta\right\} = 0 \tag{8d}$$

When $x < \beta/2$, it is possible for signal Δ_1 or Δ_2 or both to be larger than xK; when $\beta/2 \leqq x \leqq \beta$ it is possible only for either signal Δ_1 or Δ_2 (but not both) to be larger than xK.

Figure 10 represents these probability distributions for several normalized integration periods β and unity signal current $K = 1$. It may be noted that equation (8a) properly reduces to equation (7a) for $x = 0$, thus giving the probability of generating two star signals; and, similarly, equation (8c) reduces to equation (7d) for $x = 0$, thus giving the probability of generating at least one star signal.

Probability density.- The probability-density function of a continuous random variable, in this case x, is defined as the derivative of the cumulative probability distribution. (Because the distributions given by eqs. (8) increase with decreasing x, the negative value of the derivative must be used here; i.e., $p(x) = -dP(x)/dx$.) Consequently, the density functions corresponding to equations (8) are given as follows:

17
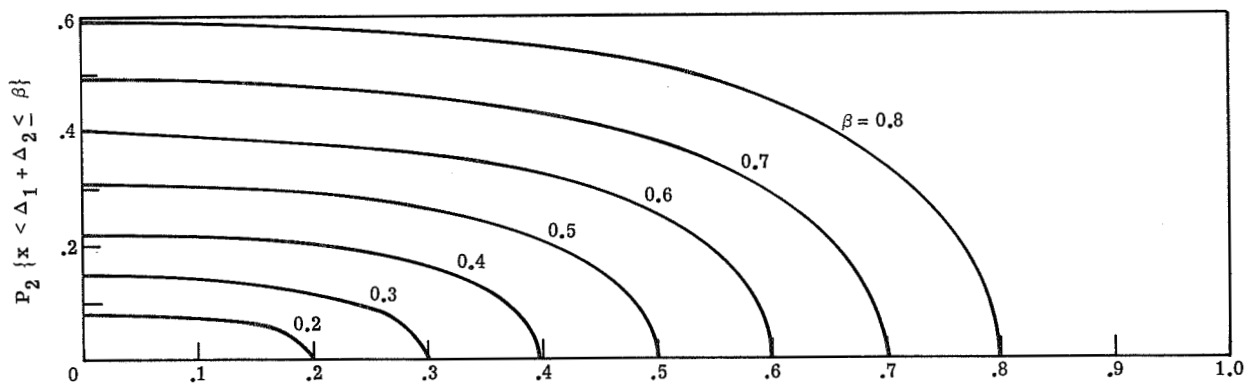
(a) Probability that the sum of two star samples is larger than x.
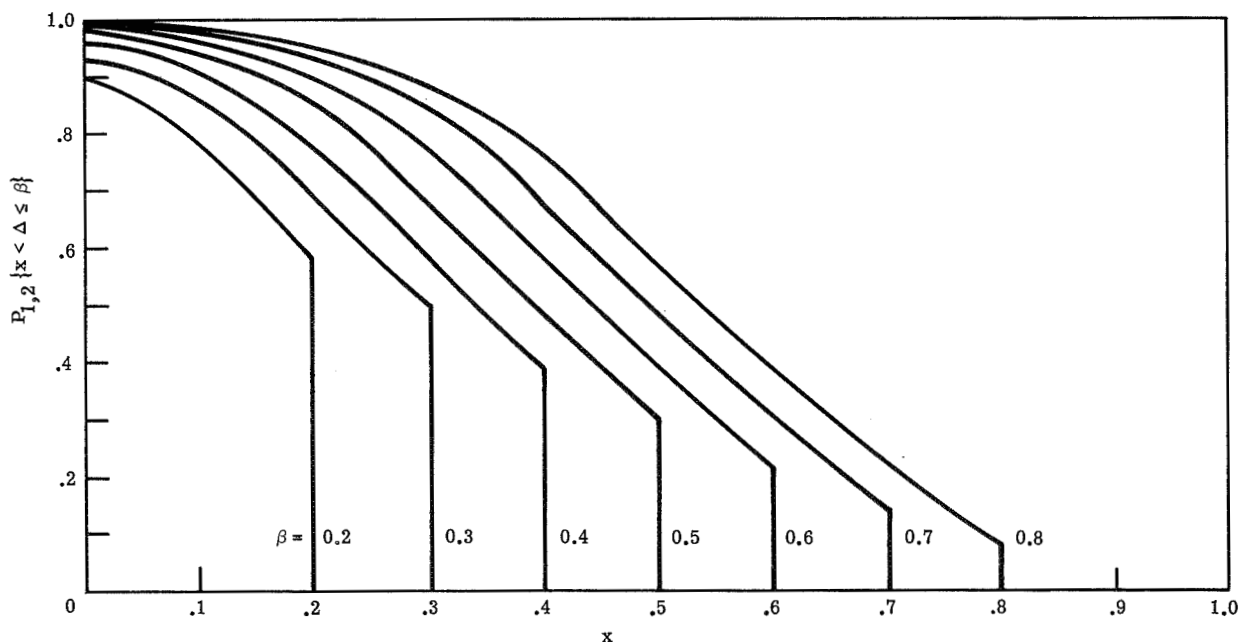
(b) Probability that at least one star sample is larger than x.

Figure 10.- Cumulative probability distribution of star samples for several values of normalized integration periods β.

(1) The sum of two star samples:

$$p_2\left\{x; \left(\Delta_1 + \Delta_2\right)\Big/K\right\} = \frac{x(\alpha + x)}{\sqrt{1 - (\alpha + x)^2}}\ \theta(\beta - x) \tag{9a}$$

where $\theta(x) = 1$ if $x > 0$ and $\theta(x) = 0$ if $x \leqq 0$.

18

(2) At least one star sample:

$$p_{1,2}(x;\Delta/K) = \frac{2 + \beta x - 3x^2}{\sqrt{1 - x^2}} - 2\sqrt{1 - (\alpha + 2x)^2} \qquad (x < \beta/2)$$

$$p_{1,2}(x;\Delta/K) = \frac{2 + \beta x - 3x^2}{\sqrt{1 - x^2}}\, \theta(\beta - x) + \frac{1}{2}\left(\cos^{-1}\beta - \beta\sqrt{1 - \beta^2}\right)\delta(x - \beta) \qquad (\beta/2 \leqq x \leqq 1)$$

$$\text{(9b)}$$

Figure 11 presents these probability densities for several normalized integration periods β and unity signal current $K = 1$. It may be noted that the impulse function represents the probability that a star signal current is integrated over the complete integration interval $0 \leqq x \leqq 1$.

Average value.- The average, or expected, value of a random occurrence, in this case the probability density function $p(x)$, is defined as

$$\bar{x} = \int_{-\infty}^{\infty} x p(x)\, dx$$

Consequently, the average values of the occurrences described by equations (9) are given as follows:

(1) The sum of two star samples:

$$\bar{x}_2\left(\Delta_1 + \Delta_2\right) = \alpha\, \sin^{-1}\alpha + \frac{1}{3}\left(2 + \alpha^2\right)\sqrt{1 - \alpha^2} - \frac{\pi}{2}\,\alpha \qquad \text{(10a)}$$

(2) At least one star sample:

$$\bar{x}_{1,2}(\Delta) = \frac{\pi}{4}\,\beta \qquad \text{(10b)}$$

Figure 12 presents the variation of these average values with the normalized integration period β; the signal current is assumed to be unity, that is, $K = 1$.
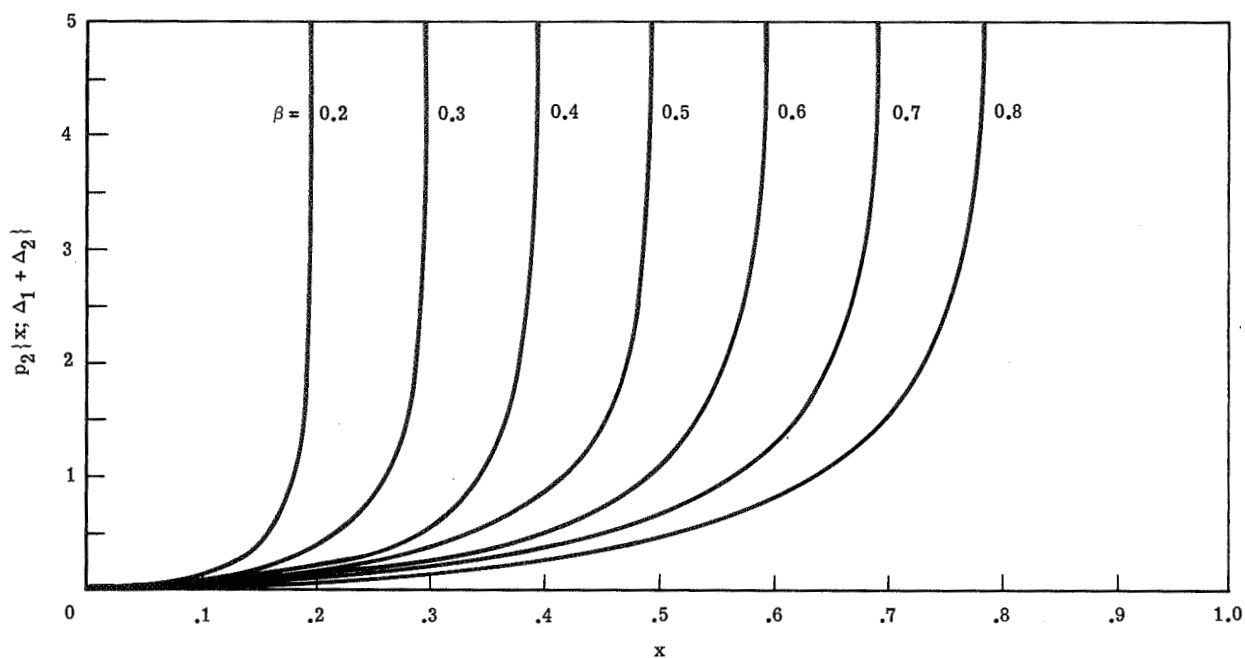
(a) Sum of two star samples.
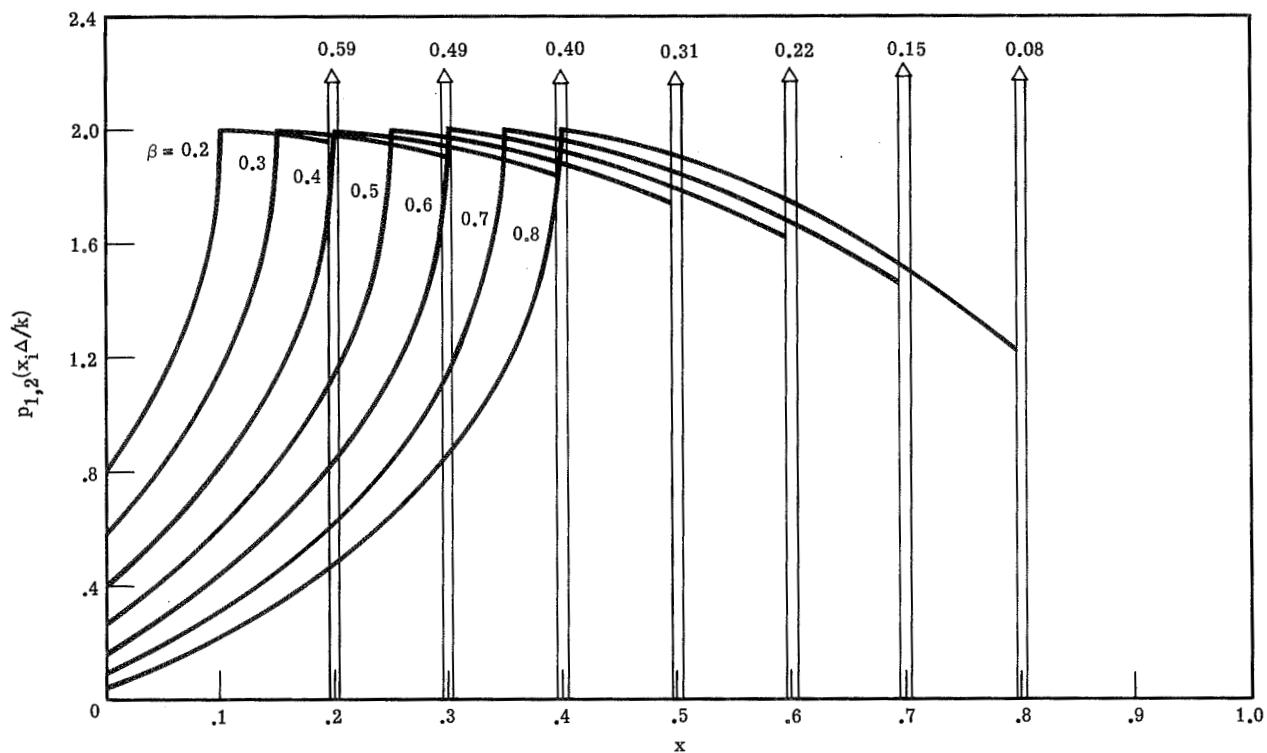
(b) At least one star sample.

Figure 11.- Probability-density function of star samples for several values of normalized integration period β.

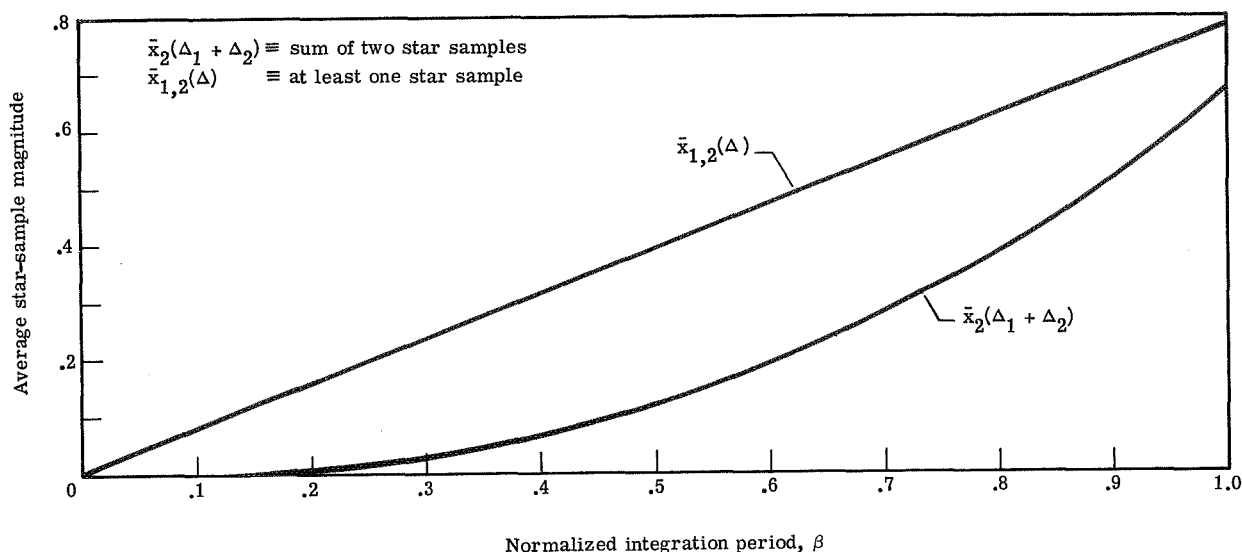Figure 12.- Variation of average star-sample magnitude plotted against integration period for $K = 1$.

DETECTION AND FALSE ALARM

Besides converting radiant power into an electrical signal current and amplifying it, the camera photosensor and preamplifier also generate a noise current. This section determines the probability of detecting star signals which are characterized by the statistics formulated in the foregoing section and are masked by this noise.

General

Based on the foregoing results, the imagery data contained in a single line scan may be searched for two signals, one signal, or at least one signal of a single star. The latter approach has the highest probability of success and is, therefore, pursued here. For simplicity, analytical results are evaluated only for signal integration intervals equal to one-half of the sampling interval (i.e., for $\alpha = \beta = 0.5$), as is the case for the Viking lander cameras.

By using a standard statistical approach (see, for example, ref. 7), the following simple hypotheses may be set up for each signal sample or picture element (pixel):

$H_0 : n$

$H_1 : s + n$

In words, hypothesis H_0 stipulates that only noise is present, and hypothesis H_1 stipulates that a star signal is also present.

21

The noise generated by the photosensor and preamplifier is random and can be expressed by the Gaussian density function (ref. 5) as

$$p_n(x) = \frac{1}{\sqrt{2\pi}\sigma} e^{-x^2/2\sigma^2} \tag{11}$$

where σ is the root-mean-square (rms) value of the noise current (in amperes).

The probability density for signal plus noise $p_{1,2,n}(x)$ is given by the convolution of the signal and noise probability density functions and can be written as

$$p_{1,2,n}(x) = p_{1,2}(x) * p_n(x) \tag{12}$$

where $p_{1,2}(x)$ is given by equation 9(b) and is plotted in figure 11(b). The two probability density functions $p_n(x)$ and $p_{1,2,n}(x)$ for hypotheses H_0 and H_1, respectively, are illustrated in figure 13.
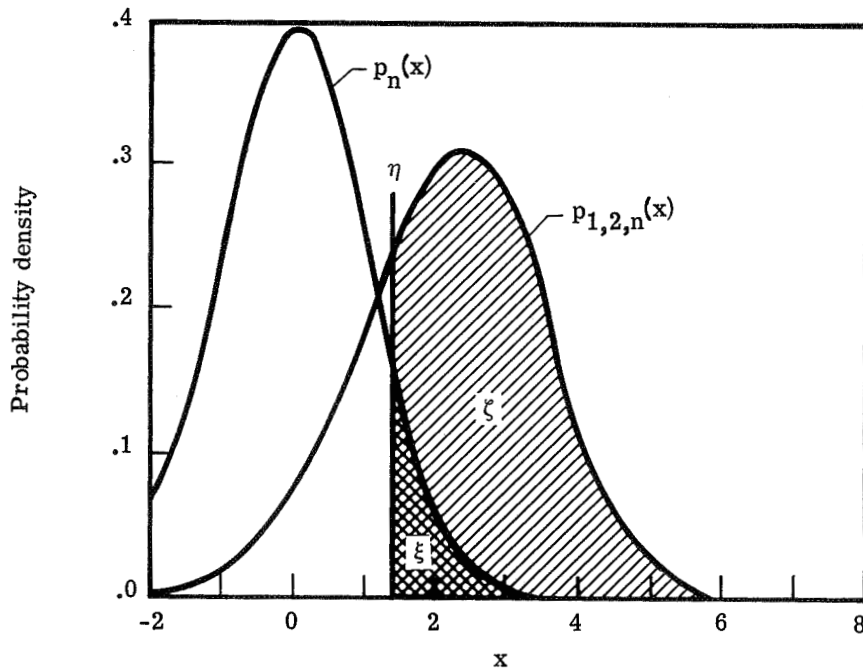

Figure 13.- Probability density of noise and signal plus noise for a signal-to-noise ratio of $K/\sigma = 6$. Also illustrated is the probability of star detection ζ and false alarm ξ for a threshold η. Normalized signal-integration period of $\beta = 0.5$.

Let it be assumed now that for any signal current x smaller than or equal to some threshold value η (i.e., $x \leqq \eta$), as illustrated in figure 13, H_0 is accepted, and that for $x > \eta$, H_1 is accepted. The probability of accepting H_1 when H_1 is, in fact, true is given by

$$\zeta = \int_{\eta}^{\infty} p_{1,2,n}(x) \, dx \tag{13}$$

Similarly, the probability of accepting H_1 when H_0 is true is given by

$$\xi = \int_{\eta}^{\infty} p_n(x) \, dx \tag{14}$$

The probability ζ, often called the power of the test, is referred to in this paper as the probability of detecting a star; the probability ξ, often called the level or size of the test, is referred to as the probability of false alarm.

Since signal plus noise are digitized for transmission as n binary digit (n-bit) words, the threshold value η is forced to be one of 2^n discrete levels. In the Viking lander cameras, for example, $n = 6$ and the spacing between quantum levels is selected by gain settings.

It should be noted that

$$\int_{-\infty}^{\infty} p_{1,2,n}(x) \, dx = \int_{-\infty}^{\infty} p_{1,2}(x) \, dx = P_{1,2}\{\Delta > 0\} = 1 - P_0\{\Delta = 0\}$$

where $P_{1,2}\{\Delta > 0\}$ is the probability that at least one star signal will be generated, and $P_0\{\Delta = 0\}$ is the probability that no star signal will be generated; both probabilities are given by equations (7). Consequently, the probability that a star which is present will not be detected is $P_{1,2}\{\Delta > 0\} - \zeta$ or $1 - \zeta - P_0\{\Delta = 0\}$.

No single approach for searching for a star signal in a set of image data may prove consistently superior to another. Nevertheless, it appears to be generally advantageous to obtain several successive line scans across a star, display this set of line scans contiguously and carefully registered, and then search for a line pattern across the line scans. Successive line scans across a star may be obtained by allowing the facsimile-camera azimuth rotation to overtake slowly the apparent star motion (due to planetary rotation), or vice versa. The Viking lander cameras also have a so-called repeated line-scan mode

which inhibits azimuth rotation without otherwise changing the camera imaging process, thus providing another opportunity to obtain several line scans across a star. If successive line scans across a star can be obtained, then the approximate slope of the line pattern may possibly be estimated from considerations of apparent star motion with respect to the camera scanning rate and geometry. If this approach is pursued, then the most useful a priori information may well be the probability of detecting at least one star signal and at least one false alarm in each one of the line scans.

Since it was assumed that only one star with sufficient irradiance to be detectable is present with a selectable field of view, or set of image data, the probability of detecting at least one star signal in a single line scan is given by equation (13). This probability is plotted in figure 14 for several threshold ratios η/σ against the signal-to-noise ratio K/σ.
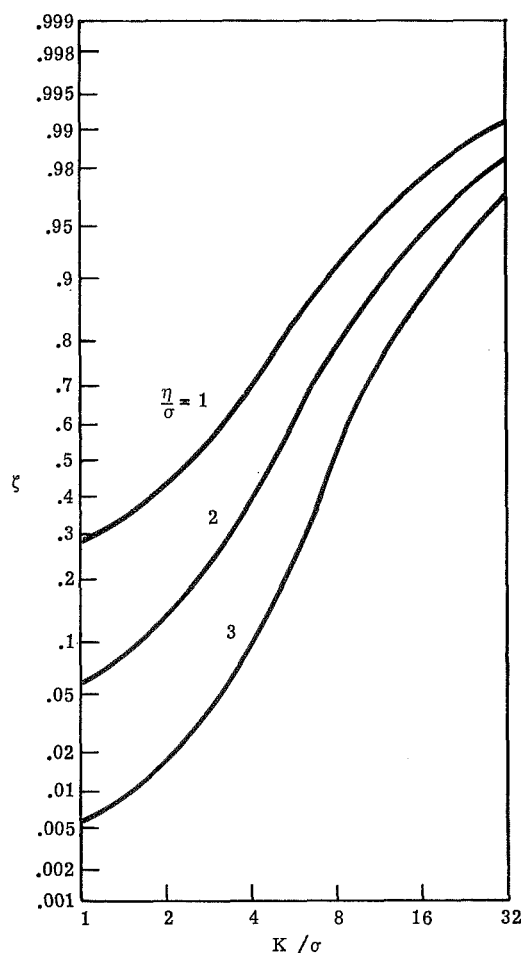
Figure 14.- Probability of detecting at least one star signal within a single line scan plotted against signal-to-noise ratio for several thresholds η/σ. Normalized signal-integration period of $\beta = 0.5$.

A false alarm, however, can occur at each pixel in the line scan. These occurrences are independent events and may be recognized as an example of Bernoulli trials (ref. 8). Thus, the probability of detecting i false alarms in N pixels is given by

$$\xi_i = \frac{N!}{(N - i)!\,i!} \, \xi^i (1 - \xi)^{N-i} \tag{15}$$

and of detecting at least one false alarm is given by

$$\sum_{i=1}^{N} \xi_i = 1 - (1 - \xi)^N \tag{16}$$

where ξ is given by equation (14). The latter probability is plotted in figure 15 for the same threshold ratios η/σ as used in figure 14.

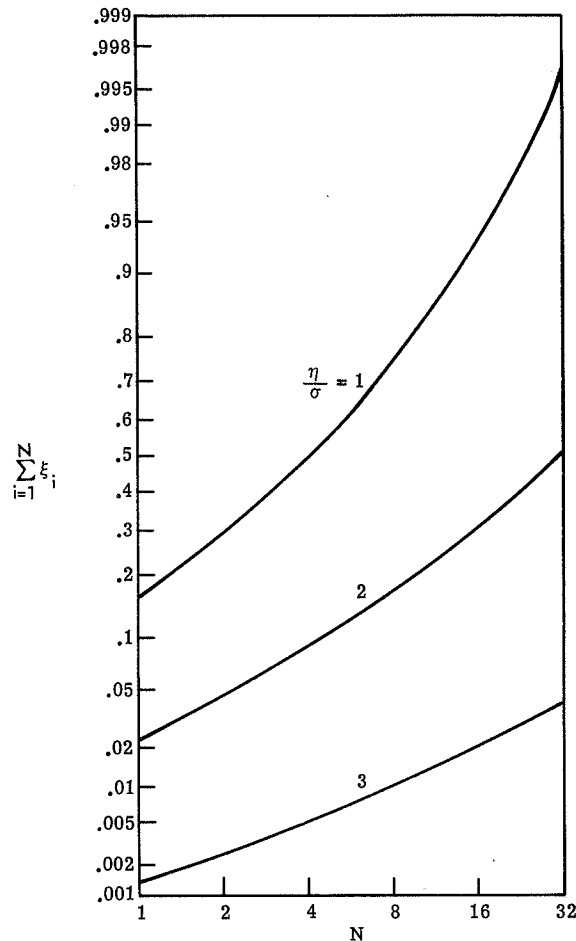Figure 15.- Probability of at least one false alarm in N pixels for several thresholds η/σ.

Application

In order to estimate the probability of detecting one of the brighter stars, it is necessary only to look up the normalized signal current K' from table I, calculate the actual signal current $K = A_c \tau_c K'$ as given by equation (5), measure the camera photosensor and preamplifier rms noise current σ, and enter the signal-to-noise ratio K/σ into figure 14. Consider the Viking facsimile-camera design (ref. 1). The objective lens-aperture diameter is 0.95 cm and the total optical transmissivity is 0.7, so that $A_c \tau_c = 0.5$ cm^2. Hence, from table I, the signal current, for example, for the star Canopus becomes $K = (0.5)(0.28 \text{ pA}) = 0.14$ pA. The total noise current of the photosensor and preamplifier may be taken as $4 \text{ fA}/\sqrt{\text{Hz}}$ (ref. 9), so that $\sigma = 0.02$ pA for the 25 Hz bandwidth of the camera slow-scan mode. Hence, the signal-to-noise ratio is $K/\sigma = 0.14/0.02 = 7$. Entering this ratio into figure 14 yields a probability of detection of about 0.7 for a threshold of $\eta/\sigma = 2$.

In order to estimate the probability of false alarm from figure 15, it is necessary only to determine the number of pixels per line scan N (i.e., vertical field of view divided by instantaneous field of view) which may be expected to contain a star signal from astronomical considerations. For example, for $N = 8$ pixels per line scan, the probability of at least one false alarm is almost 0.2 for a threshold of $\eta/\sigma = 2$. The effect of data transmission errors on false alarm is formulated in appendix C.

CONCLUDING REMARKS

The facsimile-camera response to a radiant point source, such as a star, was formulated and shown to result in a statistical rather than deterministic signal. The signal statistics were derived by using several simplifying assumptions, of which the most constraining one is that the lens point spread function is small compared to the photosensor aperture and can be neglected. Probable signal magnitudes were determined for the brighter visual and red stars, by assuming that the facsimile camera uses a silicon photosensor. Since these signals are masked by photosensor and preamplifier noise, their probability of detection and the associated probability of false alarms were also formulated and evaluated. Curves are presented which depict these probabilities for several threshold signal-to-noise ratios.

Langley Research Center,
    National Aeronautics and Space Administration,
        Hampton, Va., October 15, 1973.

APPENDIX A

LIGHT DISTRIBUTION OF A POINT-SOURCE
IMAGE NEAR FOCUS

This paper assumes that the image of a point source is essentially a delta or impulse function in the photosensor-aperture plane. This assumption cannot strictly be true, of course, because of diffraction at the objective lens, and it is further violated when defocus blur is present. The purpose of this appendix is threefold: first, to illustrate the actual size of an error-free diffraction image of a point source near the lens focal point; second, to suggest an approach which would account for an extended image of a point source; and third, to discuss the effect of the assumption of a point-source image on the results presented in this paper.

The light distribution near focus in an error-free diffraction image is given in reference 10. For the present purpose it may be sufficient to consider the total illumination of a point-source image which would fall within a circular aperture of radius v centered on the lens optical axis at a distance u from the lens focal point. Figure 16 presents a contour line for a somewhat arbitrarily selected radius v which would contain 80 percent of the total illumination. The normalized defocus distance is given by (see refs. 10 and 11)

$$u = \frac{2\pi}{\lambda}\left(\frac{D}{2l}\right)^2 \Delta l \tag{A1}$$

where D is the lens-aperture diameter, l is the photosensor-aperture distance from the lens, and Δl is the photosensor-aperture distance from geometric focus. For comparison with the radius v, the normalized photosensor-aperture radius of the facsimile camera is given by

$$v_c = \frac{2\pi}{\lambda}\left(\frac{D}{2l}\right)R_c \tag{A2}$$

where R_c is the actual photosensor-aperture radius.

Consider now the design parameters of the Viking lander camera (ref. 1) listed as follows:

Lens focal length, f, cm	5.25
Lens-aperture diameter, D, cm	0.95
Photosensor-aperture radius, R_c, μm[a]	19.0
Photosensor-aperture distance from lens, l, cm[b]	5.27
Photosensor-aperture distance from geometric focus for a point source located at infinity, Δl, cm[b]	0.02

[a]For the high-resolution photosensors; the low-resolution photosensor apertures are three times wider.

[b]For the high-resolution photosensor closest to the lens focal point.

Substituting the foregoing parameters into equations (A1) and (A2) yields $v_c \cong 15$ and $u \cong 15$ for the average wavelength of the silicon photosensor, $\lambda = 0.7$ μm.
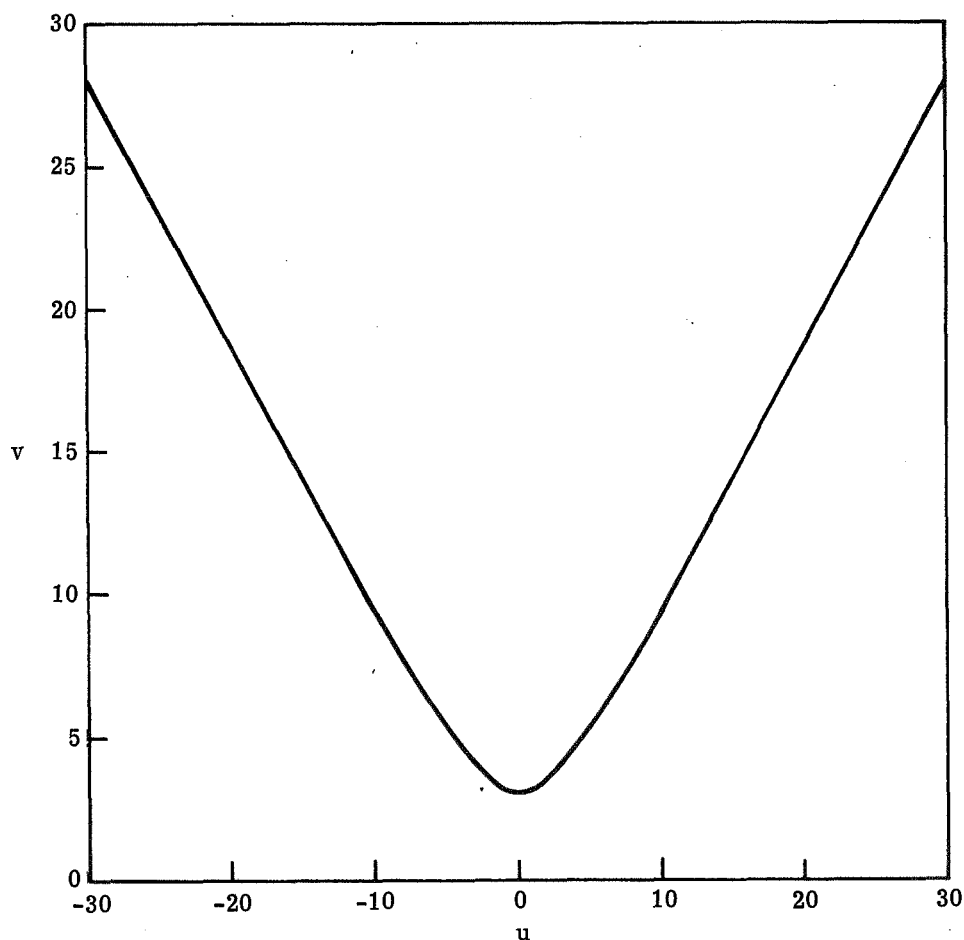

Figure 16.- Contour line for 80 percent of total illumination of a point-source image which falls within circles of radius v centered on the lens optical axis at distance u from the lens focal point (from ref. 10).

28

Figure 16 shows that $v = 3$ for $u = 0$ and that v is, therefore, less than one-fifth of the photosensor-aperture radius v_c. Thus, the assumption of a point-source image should yield fairly accurate results for this imaging situation.

As can also be seen from figure 16, $v \simeq 14$ for $u \simeq 15$ so that v is then approximately equal to v_c. Thus, the assumption of a point-source image is no longer proper, and some of the results presented in this paper are not valid for this imaging situation.

One approach to account for defocus blur would be to convolve the defocused lens point spread function (given, for example, in refs. 10 and 11) with the photosensor-aperture point spread function as formulated by equation (1), and to use the resulting function as the effective (and enlarged) photosensor-aperture point spread function. The image of a point source may then again be regarded as a delta function, and the signal statistics may be derived as outlined in the paper and detailed in appendix B.

Upon some reflection it may be visualized that the effectively "enlarged" photosensor aperture would now allow more than two signal samples of a single point source to be generated within a single line scan. The signal statistics presented in figures 9 to 12 would, therefore, significantly change — but with one important exception. This exception pertains to the probabilities associated with the generation and detection of at least one star signal. For the Viking lander camera, for which the normalized integration period β is equal to 0.5 (as used for figs. 13 and 14), the probability of generating at least one star signal (see fig. 9) is 0.98. This probability could not, of course, be significantly improved upon. Consequently, the final result presented in figure 14 — the probability of detecting at least one star signal — is not expected to change significantly in the presence of some defocus blur. The results presented in figure 15 — the probability of at least one false alarm — do not depend on any of these considerations.

APPENDIX B

DERIVATION OF SAMPLED-SIGNAL-CURRENT
STATISTICS FOR POINT OBJECTS

The purpose of this appendix is to present in detail the derivation of some of the statistics which are used in this paper to describe the sampled signal current generated by point objects. The number of star signals obtained and their magnitude depend, as previously described in the paper and illustrated in figure 8, on two independent events: (1) where (along the azimuth direction) the star signal passes across the aperture center, and (2) when (along the vertical scan direction) the star image passes across the photosensor aperture with respect to the time of integration. The signal statistics derived here are (a) the probability of generating two, one, or no signal sample, and (b) the cumulative probability distribution of the integrated and sampled-signal magnitudes. The latter statistics, (b), may be more clearly defined as the probability that at least one star sample (or the sum of two star samples) is larger than some value x, where x is an independent variable. It follows from this definition that (b) reduces to (a) for x = 0. However, since the purpose of this appendix is primarily to show how the sampled-signal statistics were derived, it is convenient to derive first (a) and then (b).

All assumptions and constraints are stated in the main part of this paper, together with illustrations of the results. Two exceptions are made for this appendix: (1) Instead of requiring that the effective vertical angular sampling interval X be equal to the circular photosensor diameter 2ρ, it is allowed that $X \geq 2\rho$; and (2) the signal current K is assumed to be unity for convenience of notation.

Probability of Generating Two, One, or No Signal Sample

Two situations may be recognized from figure 8: (1) When $\Delta\chi_i > X - \dot{\chi}_s T$, then either two or one star samples occur; and (2) when $\Delta\chi_i \leq X - \dot{\chi}_s T$, then either one or no star sample occurs. For any rectangular section i for which $\Delta\chi_i > X - \dot{\chi}_s T$, the probability of obtaining two star signals is given by

$$P_{2,i}\left\{\Delta_1>0, \Delta_2>0\right\} = \frac{1}{X}\int_0^{\Delta\chi_i+\dot{\chi}_s T-X} d\chi = \frac{1}{X}\left[\Delta\chi_i - \left(X - \dot{\chi}_s T\right)\right] \tag{B1}$$

and of obtaining one star signal is given by

$$P_{1,i}\left\{\Delta>0\right\} = \frac{1}{X}\int_{\Delta\chi_i+\dot{\chi}_s T-X}^X d\chi = \frac{1}{X}\left[\left(2X - \dot{\chi}_s T\right) - \Delta\chi_i\right] \tag{B2}$$

Similarly, for any section i for which $\Delta\chi_i \leqq X - \dot{\chi}_s T$, the probability of obtaining one star signal is given by

$$P_{1,i}\{\Delta>0\} = \frac{1}{X}\int_0^{\dot{\chi}_s T + \Delta\chi_i} d\chi = \frac{1}{X}\left(\Delta\chi_i + \dot{\chi}_s T\right) \tag{B3}$$

and of obtaining no star signal is given by

$$P_{0,i}\{\Delta=0\} = \frac{1}{X}\int_{\dot{\chi}_s T + \Delta\chi_i}^X d\chi = \frac{1}{X}\left[\left(X - \dot{\chi}_s T\right) - \Delta\chi_i\right] \tag{B4}$$

Now, let $1 \leqq i \leqq n - 1$ be the range for which $\Delta\chi_i > X - \dot{\chi}_s T$, and let $n \leqq i \leqq m$ be the range for which $\Delta\chi_i \leqq X - \dot{\chi}_s T$. The summation of all rectangular sections over the complete photosensor aperture may then be expressed as

$$P_2\{\Delta_1>0,\Delta_2>0\} = \frac{\Delta\psi}{X\rho}\sum_{i=1}^{n-1}\left[\Delta\chi_i - \left(X - \dot{\chi}_s T\right)\right] \tag{B5}$$

$$P_1\{\Delta>0\} = \frac{\Delta\psi}{X\rho}\left\{\sum_{i=1}^{n-1}\left[\left(2X - \dot{\chi}_s T\right) - \Delta\chi_i\right] + \sum_{i=n}^m \left(\Delta\chi_i + \dot{\chi}_s T\right)\right\} \tag{B6}$$

$$P_0\{\Delta=0\} = \frac{\Delta\psi}{X\rho}\sum_{i=n}^m\left[\left(X - \dot{\chi}_s T\right) - \Delta\chi_i\right] \tag{B7}$$

It follows from the foregoing definition for n that

$$\Delta\chi_n = X - \dot{\chi}_s T$$

and from the geometry of the circular photosensor aperture that

$$\Delta\chi_n = 2\sqrt{\rho^2 - \psi_n^2}$$

$$\Delta\chi_n = 2\sqrt{\rho^2 - \left(\frac{2n - 1}{2}\right)^2 (\Delta\psi)^2}$$

Equating these two equations for $\Delta\chi_n$ and solving for n yields

$$n = \frac{1}{2} + \frac{1}{\Delta\psi}\sqrt{\rho^2 - \left(\frac{X - \dot{\chi}_s T}{2}\right)^2}$$

(B8)

It follows similarly from the foregoing definition for m that

$$\Delta\chi_m = 0$$

and from the geometry of the circular aperture that

$$\Delta\chi_m = 2\sqrt{\rho^2 - \psi_m{}^2}$$

$$\Delta\chi_m = 2\sqrt{\rho^2 - \left(\frac{2m - 1}{2}\right)^2 (\Delta\psi)^2}$$

Again, equating the two equations for $\Delta\chi_m$ and solving for m yields

$$m = \frac{1}{2} + \frac{\rho}{\Delta\psi}$$

(B9)

In the limit as $\Delta\psi$ approaches zero, the summations in the probability equations (B5) to (B7) become integrals and are given as follows:

For generating two star samples,

$$P_2\left\{\Delta_1 > 0, \Delta_2 > 0\right\} = \frac{1}{X\rho}\left[\int_0^{\overline{\psi}} 2|\chi|\ d\psi - \left(X - \dot{\chi}_s T\right)\overline{\psi}\right]$$

where

$$|\chi| \equiv \sqrt{\rho^2 - \psi^2}$$

and

$$\overline{\psi} \equiv \lim_{\Delta\psi \to 0} \psi_{n-1} \equiv \lim_{\Delta\psi \to 0} \psi_n = \sqrt{\rho^2 - \left(\frac{X - \dot{\chi}_s T}{2}\right)^2}$$

Solving this equation yields for $\alpha' \leqq 1$

$$P_2\{\Delta_1 > 0, \Delta_2 > 0\} = \frac{\rho}{X}\left(\cos^{-1}\alpha' - \alpha'\sqrt{1 - \alpha'^2}\right) \tag{B10}$$

where

$$\alpha' = \frac{X - \dot{\chi}_s T}{2\rho} = \frac{X}{2\rho}\alpha$$

By this relation, α' may exceed unity if $X > 2\rho$ since $0 \leqq \alpha \leqq 1$. Thus far it has been implicitly assumed that $\overline{\psi} \geqq 0$ or $\alpha' \leqq 1$. If $\alpha' > 1$, that is, if $X - \dot{\chi}_s T > 2\rho$, two star signals cannot be generated and, hence,

$$P_2\{\alpha' > 1\} \equiv 0 \tag{B11}$$

Similarly, for generating one star sample for $\alpha' \leqq 1$,

$$P_1\{\Delta > 0\} = \frac{1}{X\rho}\left[(2X - \dot{\chi}_s T)\overline{\psi} - \int_0^{\overline{\psi}} 2|\chi|\,d\psi + \int_{\overline{\psi}}^{\rho} 2|\chi|\,d\psi + \dot{\chi}_s T(\rho - \overline{\psi})\right]$$

where $|\chi|$ and $\overline{\psi}$ are as given previously. Solving this equation yields for $\alpha' \leqq 1$

$$P_1\{\Delta > 0\} = \frac{\rho}{X}\left[-2\cos^{-1}\alpha' - 2\alpha'\left(1 - \sqrt{1 - \alpha'^2}\right) + \frac{X}{\rho} + \frac{\pi}{2}\right] \tag{B12}$$

where α' is given previously. Also, for $\alpha' > 1$

$$P_1\{\alpha' > 1\} = \frac{1}{X\rho}\int_0^{\rho}\left(2|\chi| + \dot{\chi}_s T\right)d\psi = \frac{2\rho}{X}\left(-\alpha' + \frac{X}{2\rho} + \frac{\pi}{4}\right) \tag{B13}$$

Finally, for generating no star sample for $\alpha' \leqq 1$,

$$P_0\{\Delta = 0\} = \frac{1}{X\rho}\left[(X - \dot{\chi}_s T)(\rho - \overline{\psi}) - \int_{\overline{\psi}}^{\rho} 2|\chi|\,d\psi\right]$$

$$P_0\{\Delta=0\} = \frac{\rho}{X}\left(\cos^{-1}\alpha' - \alpha'\sqrt{1 - \alpha'^2} + 2\alpha' - \frac{\pi}{2}\right) \tag{B14}$$

and for $\alpha' > 1$,

$$P_0\{\alpha'>1\} = \frac{1}{X\rho} \int_0^\rho \left(X - \dot\chi_s T - 2|\chi|\right) d\psi = \frac{2\rho}{X}\left(\alpha' - \frac{\pi}{4}\right) \tag{B15}$$

Cumulative Probability Distribution of Signal Samples

Three cumulative probability distributions are derived: (a) the sum of two star signals when two star signals are present, (b) one star signal when two star signals are present, and (c) one star signal when one star signal is present. The distribution for one star signal when either one or two star signals are present (i.e., of at least one star signal) is the sum of cases (b) and (c).

Three situations may be recognized similarly as before:

(1) When $\Delta\chi_i > X - \dot\chi_s T + xX$, then either two or one star samples definitely occur with a total magnitude Δ (where $\Delta = \Delta_1 + \Delta_2$ for two samples) greater than x.

(2) When $xX < \Delta\chi_i \leqq X - \dot\chi_s T + xX$, only one star sample may occur with a signal magnitude greater than x.

(3) When $xX \geqq \Delta\chi_i$, no star sample can occur with a signal magnitude greater than x.

The condition of two star samples in case (1) may be separated into two distinct parts: (1a) When $\Delta\chi_i > X - \dot\chi_s T + 2xX$ and two star samples occur, a portion of the interval X has both signals Δ_1 and Δ_2 each greater than x; and (1b) when $X - \dot\chi_s T + xX < \Delta\chi_i \leqq X - \dot\chi_s T + 2xX$, then either one star sample or the other may occur with a signal greater than x but not both.

From figure 8, for any rectangular section i for which $\Delta\chi_i > X - \dot\chi_s T + xX$, the probability that there are two star samples and that the magnitude of their sum $\Delta_1 + \Delta_2$ is larger than some value x is given by

$$P_{2,i}\{x<\Delta_1+\Delta_2\leqq\beta'\} = \frac{1}{X}\int_0^{\Delta\chi_i+\dot\chi_s T-X} d\chi = \frac{1}{X}\left[\Delta\chi_i - \left(X - \dot\chi_s T\right)\right] \tag{B16}$$

and

$$P_{2,i}\{\beta'\leqq x<\Delta_1+\Delta_2\} \equiv 0 \tag{B17}$$

34

where

$$\beta' = \beta - 1 + \frac{2\rho}{X} \qquad (B18)$$

and for $\beta' \leq 0$, two samples cannot exist. The probability that there are two star samples present, at least one of which is greater than x, is given by

$$P_{2,i}\left\{x<\Delta\leq\beta'\right\} = \frac{1}{X}\int_0^{\Delta\chi_i+\dot\chi_s T-X} d\chi = \frac{1}{X}\left(\Delta\chi_i + \dot\chi_s T - X\right) \qquad (B19)$$

where $\Delta\chi_i > X - \dot\chi_s T + 2xX$, and

$$P_{2,i}\left\{x<\Delta\leq\beta'\right\} = \frac{1}{X}\left(\int_0^{\Delta\chi_i-xX-X+\dot\chi_s T} d\chi + \int_{xX}^{\Delta\chi_i+\dot\chi_s T-X} d\chi\right)$$

$$P_{2,i}\left\{x<\Delta\leq\beta'\right\} = \frac{2}{X}\left(\Delta\chi_i + \dot\chi_s T - X - xX\right) \qquad (B20)$$

where $X - \dot\chi_s T + xX < \Delta\chi_i \leq X - \dot\chi_s T + 2xX$, and finally

$$P_{2,i}\left\{\beta'\leq x<\Delta\right\} \equiv 0 \qquad (B21)$$

The probability that only one star sample is present and that the signal magnitude is larger than x is given by

$$P_{1,i}\left\{x<\Delta\leq\beta'\right\} = \frac{1}{X}\int_{\Delta\chi_i+\dot\chi_s T-X}^{X} d\chi = \frac{1}{X}\left(2X - \dot\chi_s T - \Delta\chi_i\right) \qquad (B22)$$

where $\Delta\chi_i > X - \dot\chi_s T + xX$, and

$$P_{1,i}\left\{x<\Delta\leq\beta'\right\} = \frac{1}{X}\int_{xX}^{\Delta\chi_i+\dot\chi_s T-xX} d\chi = \frac{1}{X}\left(\Delta\chi_i + \dot\chi_s T - 2xX\right) \qquad (B23)$$

where $xX < \Delta\chi_i \leq X - \dot\chi_s T + xX$, and

$$P_{1,i}\left\{\beta'\leq x<\Delta\right\} \equiv 0 \qquad (B24)$$

All rectangular sections may again be summed over the photosensor aperture. The new limits of summation may also be obtained similarly. Let $\overline{\psi}_1$, $\overline{\psi}_2$, and $\overline{\psi}_3$ denote the boundaries between the aforementioned regions (1a) and (1b), (1b) and (2), and (2) and (3), respectively. Thus,

$$\overline{\psi}_1 = \rho\sqrt{1 - \left(\frac{X}{2\rho}\right)^2 (\alpha + 2x)^2} = \rho\sqrt{1 - (\alpha' + 2x')^2}$$

$$\overline{\psi}_2 = \rho\sqrt{1 - (\alpha' + x')^2}$$

$$\overline{\psi}_3 = \rho\sqrt{1 - x'^2}$$

where $x' \equiv \frac{X}{2\rho} x$.

Furthermore, when $1 \leqq \alpha' + 2x'$ and $1 > \alpha' + x'$ $\left(\text{or equivalently } \frac{2\rho}{X} \leqq \alpha + 2x \right.$ and $\left. \frac{2\rho}{X} > \alpha + x \right)$, then $\overline{\psi}_1 \equiv 0$; when $1 \leqq \alpha' + x'$, then $\overline{\psi}_1 \equiv \overline{\psi}_2 \equiv 0$; and when $1 \leqq x'$ (or $2\rho \leqq xX$), then $\overline{\psi}_1 \equiv \overline{\psi}_2 \equiv \overline{\psi}_3 \equiv 0$.

The probability that there are two star samples and that the magnitude of their sum $\Delta_1 + \Delta_2$ is larger than some value x is given by

$$P_2\left\{x < \Delta_1 + \Delta_2 \leqq \beta'\right\} = \frac{1}{X\rho} \int_0^{\overline{\psi}_2} \left[2|\chi| - \left(X - \dot{\chi}_s T\right)\right] d\psi \qquad (\alpha' + x' < 1)$$

$$P_2\left\{x < \Delta_1 + \Delta_2 \leqq \beta'\right\} = \frac{\rho}{X}\left[\cos^{-1}(\alpha' + x') - (\alpha' - x')\sqrt{1 - (\alpha' + x')^2}\right] \qquad (\alpha' + x' < 1) \qquad \text{(B25)}$$

$$P_2\left\{x < \Delta_1 + \Delta_2 \leqq \beta'\right\} = 0 \qquad (\alpha' + x' \geqq 1) \qquad \text{(B26)}$$

and for all values of α' and x',

$$P_2\left\{\beta' \leqq x < \Delta_1 + \Delta_2\right\} \equiv 0 \qquad \text{(B27)}$$

The probability that there are two star samples present, at least one of which is greater than x, is given by

$$P_2\{x<\Delta\leq\beta'\} = \frac{1}{X\rho}\left[\int_0^{\overline{\psi}_1}\left(2|\chi| + \dot{\chi}_sT - X\right)d\psi + \int_{\overline{\psi}_1}^{\overline{\psi}_2} 2\left(2|\chi| + \dot{\chi}_sT - X - xX\right)d\psi\right]$$

$$(\alpha' + 2x' < 1)$$

$$P_2\{x<\Delta\leq\beta'\} = \frac{\rho}{X}\left[(\alpha' + 2x')\sqrt{1 - (\alpha' + 2x')^2} - 2(\alpha' + x')\sqrt{1 - (\alpha' + x')^2}\right.$$

$$\left. - \cos^{-1}(\alpha' + 2x') + 2\cos^{-1}(\alpha' + x')\right] \qquad (\alpha' + 2x' < 1) \qquad \text{(B28)}$$

$$P_2\{x<\Delta\leq\beta'\} = \frac{1}{X\rho}\int_0^{\overline{\psi}_2} 2\left[2|\chi| + \dot{\chi}_sT - X - xX\right]d\psi \qquad (\alpha' + 2x' \geqq 1; \quad \alpha' + x' < 1)$$

$$P_2\{x<\Delta\leq\beta'\} = \frac{2\rho}{X}\left[\cos^{-1}(\alpha' + x') - (\alpha' + x')\sqrt{1 - (\alpha' + x')^2}\right]$$

$$(\alpha' + 2x' \geqq 1; \quad \alpha' + x' < 1) \qquad \text{(B29)}$$

$$P_2\{x<\Delta\leq\beta'\} = 0 \qquad\qquad (\alpha' + x' \geqq 1) \qquad \text{(B30)}$$

and, finally, for all values of α' and x',

$$P_2\{\beta'\leq x<\Delta\} \equiv 0 \qquad\qquad \text{(B31)}$$

The probability that only one star sample is present and that the signal magnitude is larger than x is given by

$$P_1\{x<\Delta\leq\beta'\} = \frac{1}{X\rho}\left[\int_0^{\overline{\psi}_2}\left(2X - \dot{\chi}_sT - 2|\chi|\right)d\psi + \int_{\overline{\psi}_2}^{\overline{\psi}_3}\left(2|\chi| + \dot{\chi}_sT - 2xX\right)d\psi\right]$$

$$(\alpha' + x' < 1)$$

$$P_1\left\{x<\Delta\leqq\beta'\right\} = \frac{\rho}{X}\left[2(\alpha' + x')\sqrt{1 - (\alpha' + x')^2} + \left(-3x' - 2\alpha' +\frac{X}{\rho}\right)\sqrt{1 - x'^2}\right.$$

$$\left. - 2\cos^{-1}(\alpha' + x') + \cos^{-1}x'\right] \qquad\qquad (\alpha' + x' < 1) \qquad \text{(B32)}$$

$$P_1\left\{x<\Delta\leqq\beta'\right\} = \frac{1}{X\rho}\int_0^{\bar{\psi}_3}\left(2|\chi| + \dot{\chi}_s T - 2xX\right)d\psi \qquad\qquad (\alpha' + x' \geqq 1;\ \ x' < 1)$$

$$P_1\left\{x<\Delta\leqq\beta'\right\} = \frac{\rho}{X}\left[\cos^{-1}x' + \left(-3x' - 2\alpha' +\frac{X}{\rho}\right)\sqrt{1 - x'^2}\right] \qquad\qquad (\alpha' + x' \geqq 1;\ \ x' < 1) \qquad \text{(B33)}$$

$$P_1\left\{x<\Delta\leqq\beta'\right\} = 0 \qquad\qquad\qquad\qquad (x' \geqq 1) \qquad \text{(B34)}$$

and, finally, for all values of α' and x',

$$P_1\left\{\beta'\leqq x<\Delta\right\} = 0 \qquad\qquad\qquad\qquad\qquad\qquad\qquad \text{(B35)}$$

At the beginning of this appendix it was noted that $X \geqq 2\rho$ in order that the derivations have some generality. However, in the main part of the paper it was assumed that $X = 2\rho$. Thus,

$$\alpha' \to \alpha$$

$$\beta' \to \beta$$

$$x' \to x$$

and the pertinent equations of (B10) to (B35) become

$$P_2\left\{\Delta_1>0,\Delta_2>0\right\} = \frac{1}{2}\left(\cos^{-1}\alpha - \alpha\sqrt{1 - \alpha^2}\right) \qquad\qquad \text{(B36a)}$$

$$P_1\left\{\Delta>0\right\} = \frac{1}{2}\left(\frac{\pi}{2} + 2\beta + 2\alpha\sqrt{1 - \alpha^2} - 2\cos^{-1}\alpha\right) \qquad\qquad \text{(B36b)}$$

$$P_0\left\{\Delta=0\right\} = \frac{1}{2}\left(2\alpha + \cos^{-1}\alpha - \frac{\pi}{2} - \alpha\sqrt{1 - \alpha^2}\right) \tag{B36c}$$

$$P_2\left\{x<\Delta_1+\Delta_2\leqq\beta\right\} = \frac{1}{2}\left[\cos^{-1}(\alpha + x) - (\alpha - x)\sqrt{1 - (\alpha + x)^2}\right] \tag{B37a}$$

$$P_2\left\{\beta\leqq x<\Delta_1+\Delta_2\right\} = 0 \tag{B37b}$$

$$P_2\left\{x<\Delta\leqq\beta\right\} = \frac{1}{2}\left[(\alpha + 2x)\sqrt{1 - (\alpha + 2x)^2} - 2(\alpha + x)\sqrt{1 - (\alpha + x)^2}\right.$$

$$\left. - \cos^{-1}(\alpha + 2x) + 2\cos^{-1}(\alpha + x)\right] \qquad (x < \beta/2) \tag{B38a}$$

$$P_2\left\{x<\Delta\leqq\beta\right\} = \left[\cos^{-1}(\alpha + x) - (\alpha + x)\sqrt{1 - (\alpha + x)^2}\right] \qquad (\beta/2 \leqq x < \beta) \tag{B38b}$$

$$P_2\left\{\beta\leqq x<\Delta\right\} = 0$$

$$P_1\left\{x<\Delta\leqq\beta\right\} = \frac{1}{2}\left[2(\alpha + x)\sqrt{1 - (\alpha + x)^2} + (2\beta - 3x)\sqrt{1 - x^2} - 2\cos^{-1}(\alpha + x) + \cos^{-1}x\right] \tag{B39a}$$

$$P_1\left\{\beta\leqq x<\Delta\right\} = 0 \tag{B39b}$$

APPENDIX C

TRANSMISSION ERRORS

In addition to the camera photosensor and preamplifier noise, the imagery data are also susceptible to transmission errors. The purpose of this appendix is to formulate the effect of these errors on the probability of generating false alarms.

In general, a transmission error can change the value of an n-bit pixel word which is below the threshold value η so that it is still received below this threshold (in which case the decision that no star is present is unchanged), or so that it is received above the threshold (in which case a false alarm is generated). Similarly, a transmission error can change the value of a word which is above the threshold value η so that it is still received above this threshold (in which case the decision that a star is present is unchanged), or so that it is received below this threshold (in which case a star signal is lost). In addition, it may sometimes be possible to predict that a star signal is very unlikely to exceed a determinable upper level. Some of the most significant bits of a n-bit word can then be disregarded, thus reducing the probability of false alarm.

Only the probability of false alarm for low transmission-error rates will be considered here. The probability of false alarm is higher than the probability of losing a star signal simply because a line-scan data record contains many pixels of which only one or two represent a star signal.

Let ϵ be the probability that a binary digit (bit) is in error. Then, the probability that at least one bit of a n-bit word (or the n least significant bits of a larger word) is transmitted incorrectly is given by

$$\gamma = 1 - (1 - \epsilon)^n \qquad (C1a)$$

Generally, $\epsilon < 0.01$ and $n < 10$ so that equation (C1a) can be approximated as

$$\gamma \cong n\epsilon \qquad (C1b)$$

In words, this approximation assumes that it is very unlikely that more than one transmission error occurs in a single word.

Now, let it be assumed that a n-bit word (or the n least significant bits of a larger word) which has a magnitude below or equal to the threshold value η is transmitted. The probability that this word will then be received with a magnitude above η is given by

$$\xi_t = \epsilon n \left(\frac{n - \log_2 \eta}{n} \right)$$

$$\xi_t = \epsilon \left(n - 3.32 \log_{10} \eta \right) \tag{C2}$$

The probability that the word transmitted is, in fact, below the threshold value η is $1 - \xi$, where ξ is the probability of false alarm given by equation (14). Since this probability is independent of the probability ξ_t, the probability that a false alarm will occur because of a transmission error is given by

$$\xi' = \xi_t (1 - \xi) \tag{C3}$$

Finally, since a false alarm can result independently either because of camera noise (with probability ξ) or because of a transmission error (with probability ξ'), the probability of false alarm in any given pixel becomes

$$\xi'' = \xi' + \xi$$

$$\xi'' = \epsilon \left(n - 3.32 \log_{10} \eta \right)(1 - \xi) + \xi \tag{C4}$$

Also, the probability of at least one false alarm in N pixels becomes

$$\xi''_{1,N} = 1 - (1 - \xi'')^N \tag{C5}$$

REFERENCES

1. Mutch, T. A.; Binder, A. B.; et al.: Imaging Experiment: The Viking Lander. Icarus, vol. 16, no. 1, Feb. 1972, pp. 92-110.

2. Katzberg, Stephen J.; Huck, Friedrich O.; and Wall, Stephen D.: An Investigation of Photosensor Aperture Shaping in Facsimile Cameras. NASA TN D-6882, 1972.

3. Bracewell, Ron: The Fourier Transform and Its Applications. McGraw-Hill Book Co., c.1965.

4. Goodman, Joseph W.: Introduction to Fourier Optics. McGraw-Hill Book Co., c.1968.

5. Carlson, A. Bruce: Communication Systems. McGraw-Hill Book Co., c.1968.

6. Ramsey, R. C.: Spectral Irradiance From Stars and Planets, Above the Atmosphere, From 0.1 to 100.0 Microns. Appl. Opt., vol. 1, no. 4, July 1962, pp. 465-471.

7. Davenport, Wilbur B., Jr.; and Root, William L.: An Introduction to the Theory of Random Signals and Noise. McGraw-Hill Book Co., Inc., 1958.

8. Feller, William: An Introduction to Probability Theory and Its Applications. Vol. I. Second ed., John Wiley & Sons, Inc., c.1957, p. 135.

9. Kelly, W. Lane, IV; and Katzberg, Stephen J.: Investigation of Responsivity and Noise in a Direct-Coupled Photodetector-Preamplifier for Facsimile Cameras. NASA TN D-7338, 1973.

10. Born, Max; and Wolf, Emil: Principles of Optics. Third ed., Pergamon Press, c.1965.

11. Huck, Friedrich O.; and Lambiotte, Jules J., Jr.: A Performance Analysis of the Optical-Mechanical Scanner as an Imaging System for Planetary Landers. NASA TN D-5552, 1969.